Control of oscillation periods and phase durations in half-center central pattern generators: a comparative mechanistic analysis

Silvia Daun[a]*, Jonathan E. Rubin[a]†, Ilya A. Rybak[b]
[a]Department of Mathematics,
University of Pittsburgh, Pittsburgh, PA 15260
[b]Department of Neurobiology and Anatomy,
Drexel University, College of Medicine,
Philadelphia, PA 19129

July 8, 2008

Abstract.

Central pattern generators (CPGs) consisting of interacting groups of neurons drive a variety of repetitive, rhythmic behaviors in invertebrates and vertebrates, such as arise in locomotion, respiration, mastication, scratching, and so on. These CPGs are able to generate rhythmic activity in the absence of afferent feedback or rhythmic inputs. However, functionally relevant CPGs must adaptively respond to changing demands, manifested as changes in oscillation period or in relative phase durations in response to variations in non-patterned inputs or drives. Although many half-center CPG models, composed of symmetric units linked by reciprocal inhibition yet varying in their intrinsic cellular properties, have been proposed, the precise oscillatory mechanisms operating in most biological CPGs remain unknown. Using numerical simulations and phase-plane analysis, we comparatively investigated how the intrinsic cellular features incorporated in different CPG models, such as subthreshold activation based on a slowly inactivating persistent sodium current, adaptation based on slowly activating calcium-dependent

*phone: 412-624-6949, dauns@upmc.edu
†phone: 412-624-6157, fax: 412-624-8397, rubin@math.pitt.edu

potassium current, or post-inhibitory rebound excitation, can contribute to the control of oscillation period and phase durations in response to changes in excitatory external drive to one or both half-centers. Our analysis shows that both the sensitivity of oscillation period to alterations of excitatory drive and the degree to which the duration of each phase can be separately controlled depend strongly on the intrinsic cellular mechanisms involved in rhythm generation and phase transitions. In particular, the CPG formed from units incorporating a slowly inactivating persistent sodium current shows the greatest range of oscillation periods and the greatest degree of independence in phase duration control by asymmetric inputs. These results are explained based on geometric analysis of the phase plane structures corresponding to the dynamics for each CPG type.

1 Introduction

Animal interactions with the environment include various repetitive movements (breathing, walking, swimming, flapping, scratching, chewing, and so on) that are produced by coordinated rhythmic activities of different neural populations. As shown in many studies, these rhythmic activities are generated by central pattern generators (CPGs) - special neural networks located in the central nervous system and able to generate rhythmic neural activities in the absence of afferent feedback and rhythmic inputs from other structures [1], [2], [4], [5], [6], [8], [12], [15], [13], [14], [20], [26]. The bipartite (or half-center) model of the spinal locomotor CPG proposed by Brown [1], [2] and refined by Lundberg [11] provided an important conceptual and theoretical basis for the studies of neural control of locomotion. According to this concept, the rhythmic pattern of alternating bursts of flexor and extensor activities is produced by two symmetrically organized excitatory neural populations that drive alternating activity of flexor and extensor motoneurons and reciprocally inhibit each other via inhibitory interneurons. Recent studies of fictive locomotion in decerebrate, immobilized cat preparations provided additional evidence for a symmetrical, half-center organization of the spinal locomotor CPG as well as for a critical role of reciprocal inhibition for generation and shaping of the locomotor pattern [10], [17], [25], [38]. At the same time, the specific intrinsic neural mechanisms involved in the generation of locomotor oscillations remain largely unknown.

The important features of CPGs are their flexibility and the ability to adaptively adjust the oscillatory patterns they generate to organismal demands and current motor tasks, under control of inputs from higher centers, sensory signals, and afferent feedback. In particular, these features include the capacity to alter oscillation frequency (e.g., with a change in descending excitatory drive to the CPG) and to independently change the duration of each phase (i.e., to operate in an asymmetric regime). For example, oscillation periods observed during fictive locomotion in the decerebrate, immobilized cat evoked by sustained midbrain stimulation range from approximately 0.4-0.5 s to 1.5-1.6

s [17], [38], due perhaps to changes in the descending excitatory drive [28]. During both fictive and real locomotion, changes in the locomotor period usually involve a disproportionate change in the duration of one of the phases. For example, during normal or treadmill locomotion in cats, the shortening of the step cycle (faster walking) is provided primarily by shortening the extensor phase, whereas the flexor phase remains relatively constant [7]. During fictive locomotion (in the absence of sensory feedback), changes in cycle period are usually associated with dominant changes in either extensor or flexor phase, but not in both [38], which suggests that even in the absence of afferent feedback each locomotor phase can be independently regulated by the descending supraspinal drive.

Theoretical investigations have shown that similar half-center oscillations may be produced by many different intrinsic and network mechanisms and their combinations (e.g., [4], [8], [15], [16], [21], [30], [29], [37]). For example, half-center oscillations may emerge from two half-centers (neurons or neural populations) coupled with mutual reciprocal inhibition if the activity of each half-center undergoes some form of adaptation allowing the currently suppressed half-center to escape from inhibition at a particular moment of time, become active, and inhibit the currently active half-center, or if each half-center includes some specific features producing hyperpolarization-induced rebound activity that allows the half-centers to release from inhibition and become active after a period of suppression [29]. Alternatively, each half-center may be able to generate an intrinsic bursting activity itself, which then becomes alternating and coupled because of reciprocal inhibition between the half-centers.

Rybak et al. [25] proposed a half-center model of the spinal CPG in which locomotor oscillations were produced by an escape mechanism emerging from a combination of the dynamics of persistent sodium current (I_{NaP}) in each half-center and the reciprocal inhibition between the half-centers. With changing descending excitatory drives to each half-center, the model could reproduce the full range of locomotor periods and phase durations observed during fictive and treadmill locomotion. This computational model, however, has not been theoretically investigated in detail. Moreover, although

an involvement of I_{NaP} in locomotor rhythm generation has received some experimental support [36], [39], the proposed I_{NaP}-dependent mechanism remains hypothetical. Other oscillatory mechanisms, such as those described above, can be involved in CPG operation. Since the exact intrinsic mechanisms operating in the CPG remain unknown, we aimed to comparatively investigate the ability of several CPG models to reproduce the key features of the locomotor CPG, namely its capacity to undergo changes in oscillation frequency with change of excitatory drive and its ability to operate in asymmetrical regimes, with different phase durations produced by changing drive to one half-center.

In this paper, we focus on several reduced CPG models, including a simplified version of the I_{NaP}-based Rybak et al. [25] model. Each of these models consists of two neurons with mutually inhibitory synaptic connections, forming a half-center oscillator. The unique components of these reduced models are, respectively, a persistent (slowly inactivating) sodium current, neural adaptation based on calcium influx and calcium-dependent potassium current, and postinhibitory rebound based on low-threshold activated calcium current. In each model, we incorporate excitatory synaptic inputs from external sources representing external excitatory drives to each neuron and consider the range of oscillation periods over which each CPG can maintain oscillations as the drives to both cells are varied. The resultant oscillations in all models are relaxation oscillations, consisting of two phases in which one neuron (half-center) is active and the other neuron is silent or suppressed, with rapid transitions between these phases. The other major focus of our study was the impact of changing the drive to only one of the neurons, which was motivated by the idea that the ability to separately control phase durations would allow each CPG to operate in an asymmetric regime. Interestingly, we find that the influence of asymmetric drive on CPG dynamics is highly sensitive to the intrinsic cellular mechanisms involved in rhythm generation in each CPG. We show that CPGs formed from units incorporating a slowly inactivating persistent sodium current show the greatest range of oscillation periods and the greatest degree of independence in phase duration control by asymmetric inputs.

The paper is organized as follows. Section 2 introduces the general form of the equations for the models we consider, along with some important structural aspects. These are followed by the equations for the three specific half-center oscillation mechanisms that we consider. Since each of these examples features fast and slow timescales, we present the idea of fast and slow subsystems, and we use a fast-slow decomposition to derive conditions for the existence of periodic half-center oscillations in the singular limit. Section 3 presents our results on the effects of varying the drives to both or one of the CPG units within each half-center oscillator, and comparative analysis of the effects of drive changes upon the oscillation period and phase durations. This analysis clearly lays out the hypotheses, and implications of these hypotheses, that lead to these changes. The paper concludes with a discussion, given in Section 4, and an Appendix specifying the functions and parameter values used for simulations of the models considered.

2 CPG Models and Half-Center Oscillations

2.1 Model equations

Consider, for $i \in \{1, 2\}$, a system of ordinary differential equations of the form

$$\begin{aligned} C_m v_i' &= f_i(v_i, h_i) + g_{syn} s_j (v_{syn} - v_i) + g_{app_i}(v_{app} - v_i) \equiv F_i(v_i, h_i, s_j),\ j \neq i, \\ h_i' &= \epsilon g_i(v_i, h_i), \\ s_i' &= \alpha s_\infty(v_i)(1 - s_i) - \beta s_i, \end{aligned} \tag{1}$$

where $0 < \epsilon \ll 1$, $\alpha, \beta > 0$, and $s_\infty(v)$ is a monotone increasing function taking values in $[0, 1]$. For notational convenience, let

$$s_\infty(v) = 1/(1 + \exp((v - \theta_s)/\sigma_s)),\ \sigma_s > 0, \tag{2}$$

with a limiting case of $s_\infty(v) = H(v)$, the Heaviside step function, as $\sigma_s \downarrow 0$; however, the results here carry over to more general forms of $s_\infty(v)$. In the neuronal case, each

$v_i(t)$ represents the membrane potential, or voltage, of a cell with capacitance C_m, each h_i is an associated channel state variable, and each s_i modulates the strength of the synaptic coupling current from cell i to cell j. Note that $g_{syn}s_j > 0$, such that as long as $v_i > v_{syn}$, the coupling term gives a negative contribution to v_i'. Coupling for which $v_i > v_{syn}$ over most relevant values of v_i is called inhibitory. Also note that the interval $I_s := [0, \alpha/(\alpha+\beta)]$ is positively invariant for s, and let

$$s_{max} := \frac{\alpha}{\alpha+\beta}.$$

The final term of the voltage equation in system (1) is a cell-specific applied drive current $g_{app_i}(v_{app} - v_i)$. We take $v_{app} = 0$ mV for the remainder of the paper, corresponding to a typical reversal potential for an excitatory synaptic input.

The following assumptions will be made on system (1):

($H1$) For $i \in \{1,2\}$ and fixed $s_j \in I_s$, the v-nullcline, $\{(v_i, h_i) : F_i(v_i, h_i, s_j) = 0\}$, defines a cubic-shaped curve, composed of left, middle, and right branches, in the (v_i, h_i) phase plane.

Dropping the subscript j from s_j, denote the branches of $F_i = 0$ by $v = v_L^i(h,s)$, $v = v_M^i(h,s)$, $v = v_R^i(h,s)$, with $v_L^i < v_M^i < v_R^i$ for each (h,s) on which all three functions are defined. It is important to remember, with this notation, that the variable s corresponds to the synaptic input received by the cell, driven by the voltage of the other cell. The drive current to each cell, $g_{app_i}(v_{app} - v_i)$, is also treated as synaptic but is independent of the other cell in the network. For the analysis, in some cases, we will increase the drive to one cell only. When both cells receive the same drive, we refer to this as *baseline drive*. When the drive to one cell is increased, we refer to the drive level as *extra drive* and we mark all variables describing this cell with the $\wedge$ symbol.

($H2$) For $i \in \{1,2\}$, the h-nullcline, $\{(v_i, h_i) : g_i(v_i, h_i) = 0\}$, is a monotone curve in the (v_i, h_i) plane. For fixed $s \in I_s$, the h-nullcline intersects $F_i = 0$ at a unique point $p_{FP}(s) = (v_{FP}(s), h_{FP}(s))$.

We define a cell as *excitable* if $p_{FP}(0)$ lies on the left branch of the v-nullcline, $\{(v,h) : v = v_L(h,0)\}$. Alternatively, we say that a cell is *oscillatory* if $p_{FP}(0)$ lies on the middle branch of the v–nullcline, $\{(v,h) : v = v_M(h,0)\}$; in this case, the cell will intrinsically oscillate, yielding a reduced representation of bursting activity. Finally, a cell is *tonic* if $p_{FP}(0)$ lies on the right, most depolarized branch of the v–nullcline, $\{(v,h) : v = v_R(h,0)\}$, yielding a reduced representation of tonic spiking. We assume in this study that the two neurons we are going to couple are either both excitable, both oscillatory, or both tonic.

In a neuron, a bursting solution alternates repeatedly between silent phases of relatively constant, low voltage and active phases featuring voltage spikes, which are rapid voltage oscillations of significant amplitude. A model of the form (1) can be obtained from a model bursting neuron by omitting some spike-generating currents but maintaining a current that allows for transitions to an elevated voltage state. In this model, a bursting solution consists of an oscillation composed of silent phases, with $v_i \approx v_L^i(h,s)$, alternating with active phases, with $v_i \approx v_R^i(h,s)$.

2.2 Examples

Here we specify the differential equations for the four classes of dynamics that we consider as building blocks for a half-center oscillator. For each case, the forms of auxiliary functions and the values of parameters incorporated are given in Appendix A, and these are chosen such that assumptions $(H1)-(H2)$ hold.

2.2.1 Half-center CPG based on persistent sodium current [3]

For each cell, take

$$\begin{aligned} C_m v' &= -I_{NaP} - I_L - I_{syn} - I_{app} \\ h' &= (h_\infty(v) - h)/\tau_h(v) \\ s' &= \alpha(1-s)s_\infty(v) - \beta s, \end{aligned} \tag{3}$$

where $I_{NaP} = g_{nap} m_\infty(v) h(v - e_{na})$, $I_L(v) = g_l(v - e_l)$ and $h_\infty(v), m_\infty(v), s_\infty(v)$ are monotone, sigmoidal functions, with $h_\infty(v)$ decreasing and the others increasing with v. The first equation in (3) describes the evolution of the voltage across the cell's membrane, with capacitance C_m, in terms of a persistent sodium current (I_{NaP}), a leak current (I_L), and network (I_{syn}) and drive (I_{app}) synaptic currents. The function I_{syn} takes the form $I_{syn} = g_{syn} s(v - e_{syn})$ and the current I_{app} is described by $I_{app} = g_{app} v$, where $g_{app} > 0$ is a constant. The second equation in (3) describes the slow inactivation of the persistent sodium current. Parameters are set such that $p_{FP}(0)$ lies on $\{v = v_R(h, 0)\}$ and each cell is intrinsically tonic.

2.2.2 Half-center CPG based on postinhibitory rebound [24, 31]

The equations in this case are

$$\begin{aligned} C_m v' &= -I_T - I_L - I_{syn} - I_{app} \\ h' &= (h_\infty(v) - h)/\tau_h(v) \\ s' &= \alpha(1 - s) s_\infty(v) - \beta s. \end{aligned} \tag{4}$$

As in (3), the first equation in (4) is the voltage equation, with voltage dynamics here incorporating a low-threshold or T-type calcium current, $I_T = g_T m_\infty(v) h(v - v_{ca})$, in addition to a leak current (I_L), and network (I_{syn}) and drive (I_{app}) synaptic currents, which take the same forms as in (3). The second equation in (4) describes the slow inactivation of the calcium current; $h_\infty(v), \tau_h(v)$ are different functions here than in (3); see the Appendix. Parameters are set such that $p_{FP}(0)$ lies on $\{v = v_L(h, 0)\}$ and each cell is intrinsically excitable.

2.2.3 Half-center CPG based on neuronal adaptation (modified from [9])

In this case, we take

$$\begin{aligned} C_m v' &= -I_{Ca} - I_{ahp} - I_L - I_{syn} - I_{app} \\ Ca' &= \epsilon(-g_{ca} I_{Ca}(v) - k_{ca}(Ca - ca_{base})) \\ s' &= ((1 - s) s_\infty(v) - ks)/\tau_s \end{aligned} \tag{5}$$

The voltage dynamics, described in the first equation of (5), depend here on a calcium current, $I_{Ca}(v) = \bar{g}_{Ca}((Ca_\infty(v))^2)(v - v_{Ca})$, and a calcium-dependent potassium after-hyperpolarization (AHP) current, $I_{ahp}(v, Ca) = g_{ahp}(v - e_k)(Ca^2)/(Ca^2 + k_{ahp}^2)$, in addition to the leak and synaptic currents as previously described. The second equation in (5) describes the slow evolution of the intracellular calcium concentration, based on the inward calcium current and the deviation from a baseline calcium level, ca_{base}; the parameter g_{Ca} converts units of current to units of moles/time. Note that Ca here plays the role of the variable h in system (1).

A key component of the adaptation case is that in the absence of coupling, each cell has a unique stable critical point $p_{FP}(0)$ on the right branch of its v-nullcline, $\{v = v_R(h, 0)\}$. What distinguishes this case from the persistent sodium example described earlier is that here, $v_R(h, s)$ varies much more strongly with h, leading to a much more significant decline in voltage during the active phase, instantiating the adaptation. Moreover, the location of $p_{FP}(0)$ is at a sufficiently low voltage, relative to the synaptic threshold θ_s in equation (2), that the synaptic current generated by an active cell diminishes as the cell approaches $p_{FP}(0)$.

We consider two parameter sets for this model (see Appendix), which we call Case 1 and Case 2. These cases represent different balances of effects that result from increasing drive, as we detail further below, but in both, adaptation is a crucial component of phase transitions. Case 2 is more similar to what has previously been considered in models featuring half-center oscillations with mutual inhibition and adaptation (e.g. [27],[30],[29]), but we include both to emphasize that the adaptation mechanism supports more than one type of behavior in response to drive modulation.

2.3 Fast and slow subsystems

We will seek to establish conditions under which periodically oscillating solutions can be constructed for systems (2.2.1), (2.2.2), and (2.2.3) under $(H1) - (H2)$ and the assumptions in Section 2.2, in the singular limit of $\epsilon \downarrow 0$. Results on geometric singular perturbation theory suggest that this construction will yield the existence of nearby

oscillating solutions for $\epsilon > 0$ sufficiently small [18], although checking the details rigorously may be technically involved.

To begin the analysis, let us call the points in (v, h) space where any two branches of a cubic-shaped v-nullcline meet the *knees* of this nullcline. Specifically, under $(H1)$, for fixed $s \in I_s$, the left branch $(v_L(h, s), h)$ meets the middle branch $(v_M(h, s), h)$ in the left knee of the v-nullcline, while the middle branch meets the right branch $(v_R(h, s), h)$ in the right knee. For each $s \in I_s$, let $p_{LK}(s) = (v_{LK}(s), h_{LK}(s))$ denote the left knee of the v–nullcline and, similarly, let $p_{RK}(s) = (v_{RK}(s), h_{RK}(s))$ denote the right knee of the v-nullcline.

For system (1), there are associated fast and slow subsystems. The fast subsystem is obtained by setting $\epsilon = 0$ directly and thus takes the form

$$\begin{aligned} v_i' &= F_i(v_i, h_i, s_j),\ j \neq i, \\ h_i' &= 0, \\ s_i' &= \alpha s_\infty(v_i)(1 - s_i) - \beta s_i, \end{aligned} \tag{6}$$

where we have absorbed C_m into F_i. Recall that $i \in \{1, 2\}$, so (6) is a system of six equations.

To define various slow subsystems, set $\tau = \epsilon t$ and let "dot" denote differentiation with respect to τ. Under this rescaling of time, system (1) becomes, with $i \in \{1, 2\}$,

$$\begin{aligned} \epsilon \dot{v}_i &= F_i(v_i, h_i, s_j),\ j \neq i, \\ \dot{h}_i &= g_i(v_i, h_i), \\ \epsilon \dot{s}_i &= \alpha s_\infty(v_i)(1 - s_i) - \beta s_i. \end{aligned} \tag{7}$$

The slow subsystems are obtained from system (7) by setting $\epsilon = 0$, solving the algebraic equations, and inserting the results into the h-equation. This process yields, for each $i \in \{1, 2\}$,

$$\dot{h}_i = g_i(v_X(h_i, s_j), h_i),\ j \neq i, \tag{8}$$

for $X \in \{L, M, R\}$. In equation (8), s_j depends on v_j and hence is a function of h_j.

Consider the limit of $\sigma_s \downarrow 0$ in equation (2). Since the branch $v_M(h, s)$ is unstable with respect to the fast subsystem, there are four distinct slow subsystems (8) that could theoretically be relevant. Two of these are obtained when cell i is silent and cell j active for $i = 1$ or $i = 2$, and each of these takes the form

$$\dot{h}_i = G_L(h_i) := g(v_L(h_i, s_{max}), h_i), \tag{9}$$

$$\dot{h}_j = G_R(h_j) := g(v_R(h_j, 0), h_j). \tag{10}$$

The other two subsystems involve the cases that both cells are silent or active, but we will not write these explicitly as it turns out that they will not be needed here.

A key point is that the singular solution consists of a concatenation of solutions of systems (6) and (9)-(10) for $i = 1, 2$. Projected to each (v, h)-plane, the solutions to system (6) consist of jumps between branches of v-nullclines for different values of s, while the solutions to the slow subsystems take the form of pieces of these nullclines. Although the slow subsystems above correspond to $\sigma_s \downarrow 0$, solutions obtained in this limit persist for small $\sigma_s > 0$ for the persistent sodium and postinhibitory rebound models. In the case of adaptation, the smooth form of $s_\infty(v)$ in equation (2) becomes more important. We will address this in subsection 2.4.3.

2.4 Half-center oscillation mechanisms

In this section we present the construction of periodic singular solutions for pairs of identical cells mutually coupled with synaptic inhibition, each with dynamics governed by one of the systems given in Section 2.2, under assumptions (H1)-(H2). This construction will include the derivation of conditions for each of the four cases that are sufficient to guarantee existence of such a solution. In this section we will focus on the case that both cells have the same drive.

2.4.1 Oscillations based on persistent sodium current

Figure 1A shows the nullcline configuration and the basic periodic orbit for two neurons with persistent sodium current tuned such that, in the absence of coupling, each is tonically active. The nullclines, from top to bottom, correspond to the following sets of inputs: maximal inhibition plus baseline drive, maximal inhibition plus extra drive, baseline drive without inhibition, and extra drive without inhibition. We now want to construct a periodic singular solution under the assumption that both cells receive the same, baseline drive, such that the extra drive nullclines can for the moment be ignored.

To simplify the argument, consider the limit as $\sigma_s \downarrow 0$ in equation (2). An example of how to deal with $\sigma_s > 0$ is given in subsection 2.4.3, where its positivity is important, but taking $\sigma_s > 0$ does not affect the qualitative outcome of the arguments given here. Suppose cell 1 starts at $(v_R(h_1, 0), h_1)$ for some $h_1 \in I_R := [h_{FP}(0), h_{RK}(s_{max})]$ and cell 2 starts at $p_{LK}(s_{max})$. Cell 2 jumps up immediately and inhibits cell 1. Since $h_1 < h_{RK}(s_{max})$, the resulting inhibition immediately induces it to jump down into the silent phase. We track cells 1 and 2 under the flow of (9)-(10) until the first time that cell 2 returns to $p_{LK}(s_{max})$, say at $t = t_f > 0$. Let $\tilde{h}_1$ denote the h-coordinate of cell 1 at $t = t_f$. The existence of a periodic oscillation is guaranteed if for all $h_1 \in I_R$, $\tilde{h}_1 \in int(I_R)$, the interior of I_R.

To establish this condition, let $T_S(h_1)$ be the time cell 1 spends in the silent phase, on $\{v = v_L(h, s_{max})\}$, until it jumps up, at $p_{LK}(s_{max})$. At that moment, cell 2 will jump down if its h–coordinate lies in I_R. This will occur if $T_S(h_1) > T_A$, where T_A is defined as the time of evolution on the right branch from $(v_R(h_{LK}(s_{max}), 0), h_{LK}(s_{max}))$ to $(v_R(h_{RK}(s_{max}), 0), h_{RK}(s_{max}))$, determined by the dynamics of (10). Since $T_S(h_1)$ is a monotone decreasing function of h_1, it suffices that

$$T_S(h_{RK}(s_{max})) > T_A. \tag{11}$$

Now, if condition (11) holds, then cell 2 jumps down when cell 1 jumps up. Similarly, since at that moment the h–coordinate of cell 2 lies in the interior of I_R, it follows that

during the time it takes for cell 2 to evolve back to $p_{LK}(s_{max})$ in the silent phase under (9), the h–coordinate of cell 1 will return to the interior of I_R under (10). Thus, if we view the above process as a map on the h–coordinate for cell 1, then this map contracts I_R into the interior of I_R, and a fixed point, corresponding to a singular periodic solution, exists. Moreover, there must be at least one stable fixed point of the map, and hence a stable singular periodic solution, by this contraction result.

Finally, let $(v_R(\bar{h}_1, 0), \bar{h}_1)$ denote the position of cell 1 when cell 2 is at $p_{LK}(s_{max})$ along this periodic solution. By symmetry, which can be proved easily, the period of the oscillation is $2T_S(\bar{h}_1)$.

2.4.2 Oscillations based on postinhibitory rebound

The nullcline configuration and the basic periodic orbit for two neurons with low–threshold calcium current, tuned such that in the absence of coupling each is excitable, are shown in Figure 1B. The nullclines, from top to bottom, correspond to the same inputs as in the previous case: inibition only, inhibition plus extra drive, baseline drive without inhibition, and extra drive without inhibition.

We now want to construct a periodic singular solution under the assumption that both cells receive the same, baseline drive, such that the extra drive nullclines can be ignored. Again, for simplicity, consider $\sigma_s \downarrow 0$. Suppose cell 1 starts at $p_{RK}(0)$ and cell 2 starts at $(v_L(h_1, s_{max}), h_1)$ for some $h_1 \in I_L := [h_{LK}(0), h_{FP}(s_{max})]$. Cell 1 jumps down immediately and, because cell 2 is in I_L, the resulting fast decay of inhibition immediately releases it to jump up into the active phase. We track cells 1 and 2 under the flow of (9)-(10) until the first time that cell 1 returns to $p_{RK}(0)$, say at $t = t_f > 0$. Let $\tilde{h}_1$ denote the h-coordinate of cell 2 at $t = t_f$. The existence of a periodic oscillation is guaranteed if for all $h_1 \in I_L$, $\tilde{h}_1 \in int(I_L)$, the interior of I_L.

Similarly to subsection 2.4.1, we construct a map on the h-coordinate for cell 2. Define T_S as the time of evolution from $(v_L(h_{RK}(0), s_{max}), h_{RK}(0))$ to $(v_L(h_{LK}(0), s_{max}), h_{LK}(0))$ under (9) and T_A as the time of evolution from $(v_R(h, 0), h)$ to $p_{RK}(0)$ under (10). An analogous argument to that from subsection 2.4.1 implies that if

$$T_A(h_{LK}(0)) > T_S, \tag{12}$$

then at least one stable, symmetric fixed point, corresponding to a stable singular periodic solution, exists. If we let $(v_L(\bar{h}_1, s_{max}), \bar{h}_1)$ denote the position of cell 2 when cell 1 is at $p_{RK}(0)$ along this periodic solution, then the period of this oscillation is $2T_A(\bar{h}_1)$.

2.4.3 Oscillations based on neuronal adaptation

We focus now on oscillations based on adaptation. We consider a single parameter set (Case 1), since the arguments giving existence of half-center oscillations in both cases are identical. Figure 1C shows the nullcline configurations and the basic periodic orbit for two neurons with calcium and AHP currents tuned such that, in the absence of coupling, each cell adapts but settles to a tonically active state, as discussed in subsection 2.2.3. Note that there exists a critical point on the left branch of the inhibited nullcline. This means that an inhibited cell that evolves in the silent phase is not able to reach the left knee unless the level of inhibition changes. This cell is dependent on getting released by the cell which evolves in the active phase, in order to jump up. Choosing parameters that yield this nullcline configuration ensures that the half-center oscillation in this case truly incorporates an adaptation-based mechanism.

As above, we now construct a periodic singular solution under the assumption that both cells receive the same, baseline drive. To do so, we need to consider the slow subsystem for the adaptation case. Suppose that cell i is silent, with $v_i = v_L(Ca_i, s_j)$, and cell j is active, with $v_j = v_R(Ca_j, s_i)$. Assume that since cell i is silent, $s_i = 0$. From equations (2),(7), with Ca in place of h, we have

$$s_j = s(Ca_j) := \frac{\alpha s_\infty(v_R(Ca_j, 0))}{\alpha s_\infty(v_R(Ca_j, 0)) + \beta} \tag{13}$$

in the singular limit. Thus, the slow subsystem becomes

$$\begin{aligned} \dot{Ca}_i &= g(v_L(Ca_i, s(Ca_j)), Ca_i), \\ \dot{Ca}_j &= g(v_R(Ca_j, 0), Ca_j), \end{aligned} \tag{14}$$

for g given by the Ca-equation in system (5) and $j \neq i \in \{1, 2\}$. Of course, to be precise, even if cell i is silent, s_i will be small but nonzero. In the rest of this subsection, we assume that the inhibition from a cell shuts off when it is silent, such that $s_i = 0$ here.

We will track the dynamics of a pair of cells using system (14). Even though each s is a fast variable slaved to the corresponding Ca, it is useful to visualize the cells' trajectories in a common (Ca_i, s_j) plane, shown in Figure 2A. We emphasize here that $j \neq i$, which is appropriate since the term $s_j = s(Ca_j)$, but not the term s_i, appears in the differential equation for Ca_i. In this figure, a cell that is silent jumps up to the active phase when it hits the curve of left knees, $p_{LK}(s) = \{(v_L(Ca_{LK}(s), s), Ca_{LK}(s)) : s \in [0, s_{max}]\}$. If cell 2 jumps up from the silent phase and cell 1 jumps down from the active phase at the same time, then the trajectory of cell 2 is a vertical segment from a point on $p_{LK}(s)$ to $\{s = 0\}$, while the trajectory of cell 1 is a vertical segment up from $\{s = 0\}$ to some $\{s = \hat{s} > 0\}$. If $p_{LK}(0)$ is not too large, then $\hat{s} \approx s_{max}$, and for simplicity we take $\hat{s} = s_{max}$ in Figure 2. After such a pair of jumps, cell 2 evolves along $\{s = 0\}$ in the active phase while cell 1 evolves in the silent phase, under the dynamics of system (14).

We define (Ca_σ, σ) as the point at which the curves of fixed points and left knees intersect (see Figure 2A), and therefore Ca_σ is the minimal Ca–value at which the cell in the silent phase is able to jump up. Suppose that cell 1 starts in the active phase with $Ca_1 \in I_R := [Ca_{RK}(s_{max}), Ca_{FP}(0)]$ (and with $v_1 = v_R(Ca_1, 0)$ and $s = s(Ca_1)$ correspondingly), and that cell 2 starts in the silent phase with $(Ca_2, v_2) = p_{LK}(s_1)$, with $Ca_2 \in I_L := [Ca_\sigma, Ca_{LK}(0)]$ (and with $s_2 = 0$). We can represent our set of initial conditions as a rectangle in (Ca_1, Ca_2)-space, as shown in Figure 2B, since there is a 1-1 correspondence between s and Ca along $p_{LK}(s)$. In analogy to the previous two subsections, we track cells 1 and 2 under the flow of (14) until the first time that cell 2 returns to the curve of left knees $p_{LK}(s)$, say at $t = t_f > 0$, if this return occurs. Let $\widetilde{Ca}_1$ denote the Ca-coordinate of cell 1 at $t = t_f$ and $\widetilde{Ca}_2 = Ca_{LK}(\tilde{s}_1)$ the Ca–coordinate of cell 2 at that time. The existence of a periodic oscillation is guaranteed if t_f exists and for all $(Ca_2, Ca_1) \in R_{Ca} := I_L \times I_R$, $(\widetilde{Ca}_2, \widetilde{Ca}_1) \in int(R_{Ca})$.

Suppose that a cell is active and the inhibition it receives jumps from $s = 0$ to $s = s_{max}$. That cell will jump down if and only if its Ca–coordinate is above $Ca_{RK}(s_{max})$. Thus, the existence of a periodic solution of the type we seek will require that when each cell is active, its Ca–coordinate rises above $Ca_{RK}(s_{max})$. Hence, t_f exists if

$$\sigma > s(Ca_{RK}(s_{max})), \tag{15}$$

for $s(Ca)$ defined in equation (13), and (15) is our first existence condition. This condition could be weakened by replacing $Ca_{RK}(s_{max})$ with any value in $int(I_R)$, in which case this value would be substituted for $Ca_{RK}(s_{max})$ in the arguments below, but we neglect this possibility here for clarity.

We have assumed that, in the (Ca_i, s_j)–plane, cell 2 starts at $p_{LK}(s_1)$ for $s_1 \in [0, \sigma]$, such that $Ca_2 \in I_L$, and cell 1 starts at $(Ca_1, 0)$ with $Ca_1 \in I_R$. From this configuration, cell 2 jumps up immediately and, because cell 1 is in I_R, the resulting inhibition induces it to jump down into the silent phase. As long as (15) holds, cell 1 will eventually reach $p_{LK}(s)$ and jump up again. How long this takes to occur depends on Ca_2 at time 0, since the time course of Ca_2 controls the time course of $s(Ca_2)$, the inhibition from cell 2 to cell 1, and on the value of Ca_1. If we fix the initial $Ca_2 \in I_L$, then the amount of time it takes for cell 1 to reach $p_{LK}(s)$ is a monotonically increasing function of $Ca_1 \in I_R$, due to the slope of $p_{LK}(s)$. Define $\Phi(t; Ca)$ as the solution of the second equation of (14) with initial condition Ca. Define $T_A(Ca)$ by $\Phi(T_A(Ca); Ca) = Ca_{RK}(s_{max})$. Define $T_S(Ca)$ as the time it takes to evolve system (14) with $i = 1, j = 2$ from initial condition $(Ca_1, Ca_2) = (Ca_{RK}(s_{max}), Ca)$ until cell 1 hits $p_{LK}(s)$. Given any initial condition on R_{Ca}, it follows that cell 2 will be in position to jump down when cell 1 hits $p_{LK}(s)$ if

$$T_A(Ca_2) < T_S(Ca_2), \ \forall \ Ca_2 \in I_L. \tag{16}$$

Note that cell 1 must jump up with $Ca_1 > Ca_{LK}(0)$, since s_2 cannot actually reach 0 while cell 2 is active, and cell 2 must jump down with $Ca_2 < Ca_{FP}(0)$. Finally, given conditions (15),(16), repeating the argument one more time gives $(\widetilde{Ca}_2, \widetilde{Ca}_1) \in int(R_{Ca})$, such that a singular periodic solution exists, and numerical simulations (e.g. Figure 1C) indicate that this solution is symmetric.

	g_{app_0}	relative g_{app} range	relative T range	$\Delta T/\Delta g_{app}$
Persistent sodium	0.235	0.383	1.28	3.34
Postinhibitory rebound	0.05	1.80	0.197	0.110
Adaptation, Case 1:	0.815	0.331	0.576	1.74
Adaptation, Case 2:	0.63	1.59	0.356	0.224

Table 1: *Changes in oscillation periods and drive conductances in the balanced case.*

3 Control of Oscillation Period and Phase Durations

For each half-center oscillation mechanism, an example of the basic, or reference, periodic orbit that exists when both cells receive the same, baseline drive is shown in Figure 1. We refer to this as the balanced case. When the conductance g_{app} of the baseline drive current to both cells is varied, by an amount that is not too great, each periodic half-center solution will persist, although the period will change. If the drive is changed enough, then the number of stable states may change, and the periodic oscillation itself may be lost. We did not explore additional branches of solutions, but rather focused on the single branch of oscillations that we followed from a baseline value of g_{app}. For this branch, we computed how the half-center oscillation period varies over a range of g_{app} for each case. We display the results in Figure 3 and summarize them in Table 1. Here, g_{app_0} is defined as the midpoint of the range of g_{app} over which oscillations were observed, the relative g_{app} range is given by the total range divided by g_{app_0}, the relative T range is given by the maximal period minus the minimal period, divided by the period T_0 occurring at $g = g_{app_0}$, and $\Delta T/\Delta g_{app}$ is the relative T range divided by the relative g_{app} range. In brief, while the postinhibitory rebound mechanism yields oscillations over the greatest relative range of g_{app} values, the persistent sodium mechanism shows the greatest relative range of periods as well as the greatest sensitivity of period to changes in drive conductance.

Note from Figure 3 that the two different adaptation cases that we consider show monotone and non-monotone relationships of oscillation period to g_{app}, respectively. In Case 1, the dominant effect of increasing g_{app} is that the left knee of each nullcline is raised, due to the fact that the silent phase, but not the active phase, lies far from the

excitatory synaptic reversal potential. In Case 2, we have changed the excitatory reversal potential as well as the synaptic threshold and maximal synaptic conductance s_{max}. For relatively small g_{app}, phase transitions require substantial decay of the inhibitory conductance s. Thus, each cell jumps up to high v, with small Ca, and periods are long (Figure 4A). Increases in g_{app} induce two effects, both tied to the fact that the v-nullcline shifts up for each fixed s. As in Case 1, the rise in the left knee of the v-nullcline promotes earlier phase transitions. Additionally, however, the new excitatory reversal potential allows a more significant change in the active phase, such that at each (Ca, s), the active cell has larger v. Coupled with the voltage-dependence of s indicated in equation (2), this effect leads to stronger inhibition to the silent cell and also delays adaptation, thereby promoting longer active phase durations and period. As seen in Figure 3, the former effect dominates for small increases in g_{app}, while the latter takes over as g_{app} increases further, leading to a non-monotone dependence of period on g_{app}.

In the subsequent subsections, we consider what happens if the drive to just one cell is increased, for each half-center oscillation mechanism. We refer to this situation as the asymmetric case. Without loss of generality, we assume that cell 1 receives the additional drive, corresponding to $g_{app_1} > g_{app_2}$. Note that all variables that describe the dynamics of cell 1 are marked with the $\wedge$–symbol to distinguish these variables from the ones describing the dynamics of cell 2, the cell receiving baseline drive. For each half-center oscillation mechanism introduced in Section 2, we assume that there exists a periodic half-center oscillation (in the singular limit, at least) and we establish sufficient conditions for this type of solution to persist as drives become asymmetric. First, we consider how the silent and active phase durations for each cell change as a result of the increase in drive to one cell.

Figure 5 illustrates the changes in silent phase durations observed numerically for several values of g_{app_1} in the four analyzed cases. More specific quantitative findings are presented in Table 2. To generate this table, we defined the relative range of g_{app_1} as the range of g_{app_1} over which oscillations were maintained, divided by g_{app_0}, the midpoint of the interval of g_{app} over which periodic oscillations exist in the balanced case (as well

	g_{app_0}	rel g_{app_1} range	rel T_{S_1} range	rel T_{S_2} range	$\Delta T_{S_1}/\Delta T$
Persistent sodium	0.235	0.438	2.30	0.0167	0.993
Postinhibitory rebound	0.05	2.40	0.0582	0.181	0.243
Adaptation, Case 1:	0.815	0.270	0.544	-0.0187	1.04
Adaptation, Case 2:	0.63	1.43	0.722	-1.49	0.624

Table 2: *Changes in drive conductances and silent phase durations in the asymmetric case (rel abbreviates relative).*

as the drive to cell 2 here). Moreover, we defined the relative range of T_{S_1} (T_{S_2}) as the range of silent phase durations for cell 1 (cell 2) divided by T_{S_0}, the silent phase duration for both cells with $g_{app_1} = g_{app_2} = g_{app_0}$. Finally, $\Delta T_{S_1}/\Delta T$ denotes the observed range of T_{S_1} divided by the range of oscillation periods, which represents a measure of the phase independence, or degree to which changes in period are attributable to changes in silent phase duration for the oscillator receiving extra drive. Note that oscillations are maintained over the greatest relative range of drive asymmetries in the postinhibitory rebound model, while the greatest range of phase durations achieved by changes in drive to cell 1 is observed in the persistent sodium model, specifically in the silent phase duration for cell 1. Crucially, the persistent sodium model displays the greatest capacity for independent phase modulation, exhibiting strong changes in the silent phase duration of cell 1 and negligible changes in the silent phase duration of cell 2 when the drive to cell 1 alone is modulated; the adaptation model in Case 1 displays a rather high degree of phase independence as well, although it achieves a more limited range of oscillation periods.

Finally, Table 3 qualitatively summarizes the changes in silent and active phase durations for cells 1 and 2 shown in Figure 5. In Table 3, the number of symbols in each entry in Table 1 corresponds to the relative strength of the effect. Note that, consistent with the results with balanced drive, Case 1 of adaptation represents an intermediate case between the persistent sodium model and a strong adaptation regime, represented by Case 2 (see also subsection 3.3 and Section 4).

	cell 1 silent	cell 2 silent
Persistent sodium	- - - - -	-
Postinhibitory rebound	-	- -
Adaptation Case 1:	- - -	+
Adaptation Case 2:	- - -	++++

Table 3: *Qualitative summary of the observed changes in phase durations.*

3.1 Half-center CPG based on persistent sodium current

Recall that for the persistent sodium half-center oscillator, phase transitions occur when the cell from the silent phase reaches the appropriate left knee and jumps up to the active phase, inhibiting the cell that is already there. For the balanced case $g_{app_1} = g_{app_2}$, the single condition (11) suffices to give the existence of a stable half-center oscillation. Condition (11) ensures that when the active cell becomes inhibited, it immediately jumps down to the silent phase.

As shown in Figure 1, once $g_{app_1} > g_{app_2}$, there are four nullclines to consider for the coupled pair of cells. Nonetheless, if g_{app_1} is not increased too much, then both cells have critical points in the active phase in the absence of coupling (lower nullclines in Figure 1), corresponding to sustained tonic spiking, and the phase switches still occur when each silent cell reaches its left knee and jumps up.

Recall that we will use the symbol $\wedge$ to label structures defined for extra drive and no extra symbol to label baseline drive structures. In tracking cells during time, note that $\hat{h}_1(0)$, $h_L(0)$ refer to the cells' h–coordinates at time $t = 0$, while $h_x(0)$, $\hat{h}_x(0)$ for $x \in \{LK, RK, FP\}$ refer to the h–coordinates of various structures with inhibition $s = 0$. Suppose the cell with the extra drive (cell 1) starts in the active phase at $(\hat{v}_R(\hat{h}_1(0), 0), \hat{h}_1(0))$ and the other cell (cell 2) starts in the silent phase at $(v_{LK}(s_{max}), h_{LK}(s_{max}))$, poised to jump up (see Figure 6A). We can assume that $\hat{h}_1(0) > \hat{h}_{FP}(0)$, since $(\hat{v}_{FP}(0), \hat{h}_{FP}(0))$ is a fixed point on the right branch of the appropriate nullcline. Cell 1 will jump down when cell 2 jumps up as long as $\hat{h}_1(0) < \hat{h}_{RK}(s_{max})$. Thus, the minimum time that cell 1 spends in the silent phase is the time of evolution from $\{h = \hat{h}_{RK}(s_{max})\}$ to $\{h = \hat{h}_{LK}(s_{max})\}$ under the flow of (9), call it $\hat{T}_S^1$.

Similarly, when cell 1 jumps up, the relevant range of values for the h–coordinate of cell 2, call it $h_2(\hat{T}_S^1)$, over which cell 2 can jump down is $(h_{FP}(0), h_{RK}(s_{max}))$. Thus, one condition for the existence of a periodic half-center oscillation, in the singular limit, is $\hat{T}_S^1 > T_A^2$, where T_A^2 is the time of evolution from $\{h = h_{LK}(s_{max})\}$ to $\{h = h_{RK}(s_{max})\}$ under the flow of (10). Further, the minimum time that cell 2 spends in the silent phase is the time of evolution from $\{h = h_{RK}(s_{max})\}$ to $\{h = h_{LK}(s_{max})\}$ under the flow of (9), call it T_S^2. When cell 2 jumps up, cell 1 will be able to jump down as long as $T_S^2 > \hat{T}_A^1$, where $\hat{T}_A^1$ is the time of evolution from $\{h = \hat{h}_{LK}(s_{max})\}$ to $\{h = \hat{h}_{RK}(s_{max})\}$ under the flow of (10). In summary, the existence of a singular, periodic half-center oscillation when $g_{app_1} > g_{app_2}$ follows from a pair of conditions, $\hat{T}_S^1 > T_A^2$ and $T_S^2 > \hat{T}_A^1$, that are the natural generalization of (11). Next, we consider how the durations of various phases change as g_{app_1} is increased.

First, note that in this half-center oscillation, the silent (active) phase of cell 1 coincides with the active (silent) phase of cell 2. Thus, there are really only two changes to consider. Second, note that the key to understanding these changes is understanding how changes in g_{app} affect the v-nullcline. We now list several properties of the v-nullcline, specifically some effects on the v-nullcline achieved by varying g_{app}. To understand this discussion, recall from our original, general system of equations (1) that $F(v, h, s)$ denotes dv/dt (without loss of generality, we set $C_m = 1$). We now refer to this quantity as $F(v, h, s, g_{app})$, to make explicit the role of g_{app}. Similarly, the branches of the v-nullcline can be expressed as $v_X(h, s, g_{app})$ for $X \in \{L, M, R\}$.

($E1$) An increase in g_{app_1} causes the v-nullcline for cell 1 to shift to a lower h value for each fixed $v < 0$, and to a higher h value for each fixed $v > 0$, since we assume that the synaptic drive current reverses at $v_{app} = 0$. Importantly, the size of the shift is proportional to $v - v_{app} = v$. Thus, the greatest effects of the increase appear in the silent phase, where

$$\partial v_L(h, s, g_{app})/\partial g_{app} > 0. \tag{17}$$

($E2$) Implicit differentiation of $F(v_L(h, s, g_{app}), h, s, g_{app}) = 0$ yields

$\partial v_L/\partial h = -(\partial F/\partial h)/(\partial F/\partial v)$. Moreover, $\partial F/\partial h = -g_{NaP} m_\infty(v_L)(v_L - v_{na})$ on the left branch, where $m_\infty(v_L)$ is small, due to the deactivation of I_{NaP}. Hence, away from the left knee, where $\partial F/\partial v = 0$, we have that $|\partial v_L/\partial h|$ is small. Correspondingly, large shifts in the v-nullcline in the h direction due to changes in g_{app} are translated into much smaller changes in v_L.

($E3$) Instead of expressing the v-nullcline as $v_L \cup v_M \cup v_R$, we can instead express it as the graph of a function h_n, where $F(v, h_n(v, s, g_{app}), s, g_{app}) = 0$. The knees of the v-nullcline satisfy

$$0 = N(v, s, g_{app}) := F_v(v, h_n(v, s, g_{app}), s, g_{app}). \tag{18}$$

In particular, the left knee is given by $(v_{LK}(s, g_{app}), h_{LK}(s, g_{app}))$, where $v_{LK}(s, g_{app})$ is one solution of (18) and $h_{LK}(s, g_{app}) = h_n(v_{LK}(s, g_{app}), s, g_{app})$. Thus,

$$\partial h_{LK}/\partial g_{app} = (\partial h_n(v_{LK}, s, g_{app})/\partial v)(\partial v_{LK}/\partial g_{app}) + \partial h_n(v_{LK}, s, g_{app})/\partial g_{app}.$$

Since the knees are exactly the points where $\partial h_n/\partial v = 0$ and $\partial v_{LK}/\partial g_{app}$ is finite, this equation gives $\partial h_{LK}/\partial g_{app} = \partial h_n(v_{LK}, s, g_{app})/\partial g_{app}$. Direct calculation yields

$$\partial h_n(v_{LK}, s, g_{app})/\partial g_{app} = (-v_{LK})/(g_{nap} m_\infty(v_{LK})(v_{LK} - v_{na})). \tag{19}$$

Now, the numerator in equation (19) is bounded well above zero, since in the silent phase, including the left knee, v is significantly below zero. The denominator, however, is negative and small, reflecting the deactivation of I_{NaP} in the silent phase. Hence, the h-coordinate of the left knee decreases significantly as g_{app} increases.

We also append one additional hypothesis to this list of effects.

($H3$) With baseline drive, $h_{LK} \approx h_\infty(v_{LK})$.

Assuming $(H1) - (H2)$, effects $(E1) - (E3)$ follow, and from these and $(H3)$, we can deduce the temporal effects of changing g_{app_1}. Recall that we previously used $\bar{h}_1$ to

denote the initial h-coordinate of cell 1, in the active phase in the half-center oscillation that we proved exists in the balanced drive case. Let $h_1(t)$ denote the h-coordinate of cell 1 along this balanced half-center oscillation, with $h_1(0) = \bar{h}_1$. Suppose that in the asymmetric case, at time $t = 0$, the h-coordinate of cell 1 lies at $\bar{h}_1$ as well, and let $\hat{h}_1(t)$ denote the h-coordinate of cell 1 in the ensuing solution, also assuming, as previously, that at time 0, cell 2 lies at $(v_{LK}(s_{max}), h_{LK}(s_{max}))$. We will compare $\hat{h}_1(t)$ to $h_1(t)$. In a nutshell, we will note that when g_{app_1} is increased, one effect pushes $h_1(t)$ above $\hat{h}_1(t)$ while another does the reverse, but these effects are weak. Beyond these, the dominant effect of increasing g_{app_1} is, as stated in $(E3)$, that h_{LK} is significantly decreased, which leads to a much shorter silent phase duration $\hat{T}_S^1$ for cell 1 relative to the silent phase duration T_S of both cells in the balanced case.

To establish all of these claims, we first note that if we let time flow in the asymmetric case from the initial configuration just described, then cell 1 jumps down immediately as long as $g_{app_1} - g_{app_2}$ is not too large, since cell 2 instantly jumps up and inhibits cell 1. Cell 1 evolves on the left branch $\{v = \hat{v}_L(h, s_{max})\}$ under (9), since it receives extra drive. Since (17) holds, $v_L(h, s_{max}) < \hat{v}_L(h, s_{max})$ for each fixed h, including $h = \bar{h}_1$. Hence, $h_\infty(v_L(h, s_{max})) > h_\infty(\hat{v}_L(h, s_{max}))$ for fixed h. Thus, for small $t > 0$ at least, $\dot{h}_1(t) > \dot{\hat{h}}_1(t)$ and $h_1(t) > \hat{h}_1(t)$ follows.

This initial calculation hints that increased drive may lead to a longer residence time in the silent phase. However, this effect is quite small. Indeed $(E2)$ implies that large shifts in the v-nullcline in the h direction, corresponding to the size of $\partial h_n/\partial g_{app} = -v/(g_{nap} m_\infty(v)(v - v_{na}))$, are rescaled into much smaller shifts in v_L for each fixed h away from the knee, including $h = \bar{h}$. Moreover, another small effect works to oppose this small one. Since $\partial h_n/\partial g_{app} < 0$ from the above expression, it follows that if $h_1(t)$ gets too far ahead of $\hat{h}_1(t)$, such that $v_1(t) = \hat{v}_1(t)$, then $\dot{\hat{h}}_1(t) > \dot{h}_1(t)$, and the lead of $h_1(t)$ over $\hat{h}_1(t)$ will decrease.

Because the total effect of these factors is weak, the dominant impact of increasing g_{app_1} is its effect on the left knee, presented in $(E3)$. That is, since $\partial h_{LK}/\partial g_{app}$ is negative and has large magnitude, the net effect of increasing g_{app_1} is that $\hat{T}_S^1$ is significantly

shorter than T_S. This means that cell 1 spends a shorter time in the silent phase, and correspondingly cell 2 spends a shorter time in the active phase, in the asymmetric drive case.

The shorter active phase residence implies that cell 2 jumps down with $h_2(\hat{T}_S^1) > \bar{h}$. Thus, even though cell 2 evolves according to (9) in the silent phase, exactly as in the balanced drive case, its silent phase residence time satisfies $T_S^2 < T_S$. We note, however, that the difference between T_S^2 and T_S is very small. The small size of this change follows from two effects. First, assume that the existence conditions for the periodic half-center oscillation hold, such that $h_2(\hat{T}_S^1) \in (h_{FP}(0), h_{RK}(s_{max}))$, and that $h_{FP}(0)$ is close to $h_{RK}(s_{max})$, as in Figure 6. These assumptions constrain fairly tightly the position of h_2 at jump-down. Second, assume that property $(H3)$ holds, as also shown in Figure 6. Under this assumption, the rate of change of h_2 becomes quite slow when cell 2 is in the neighborhood of the left knee in the silent phase, and the time T_S^2 is dominated by the time spent in this neighborhood, which washes out small differences in jump up positions.

Finally, repeating the above arguments yields a sequence of successively shorter silent phase durations for each cell. Both sequences must converge, if the existence conditions for a half-center oscillation are satisfied. If $(H1) - (H3)$ hold and these conditions are satisfied, then effects $(E1) - (E3)$, which we have shown to be inherent in the persistent sodium half-center oscillation mechanism, imply that the silent phase duration for cell 1 (and active phase duration for cell 2) ends up much shorter than in the balanced drive case, due predominantly to the change in knee positions specified in $(E3)$, while the silent phase duration for cell 2 (and active phase duration for cell 1) is only very slightly decreased (see Figure 6 B).

3.2 Half-center CPG based on postinhibitory rebound

For the postinhibitory rebound half-center oscillator, phase transitions occur when the cell from the active phase reaches the appropriate right knee and jumps down into the silent phase, releasing the cell that is already there to jump up into the active phase. For

the balanced case $g_{app_1} = g_{app_2}$ the single condition (12) suffices to give the existence of a stable half-center oscillation. Condition (12) ensures that when the silent cell becomes released, it immediately jumps up to the active phase.

As shown in Figure 1 and Figure 7A, once $g_{app_1} > g_{app_2}$, there are four nullclines to consider for the coupled pair of cells. Nonetheless, if g_{app_1} is not increased too much, then both cells have critical points in the silent phase in the absence of coupling (upper nullclines in Figure 1), and the phase switches still occur when each active cell reaches its right knee and jumps down.

As in Section 3.1, the existence of a singular, periodic half-center oscillation when $g_{app_1} > g_{app_2}$ follows from a pair of conditions, $T_A^2 > \hat{T}_S^1$ and $\hat{T}_A^1 > T_S^2$, that are the natural generalization of (12). Here, T_A^2 is the time of evolution from $\{h = h_{LK}(0)\}$ to $\{h = h_{RK}(0)\}$ under the flow of (10), $\hat{T}_S^1$ is the time of evolution from $\{h = \hat{h}_{RK}(0)\}$ to $\{h = \hat{h}_{LK}(0)\}$ under the flow of (9), $\hat{T}_A^1$ is the time of evolution from $\{h = \hat{h}_{LK}(0)\}$ to $\{h = \hat{h}_{RK}(0)\}$ under the flow of (10), and T_S^2 is the time of evolution from $\{h = h_{RK}(0)\}$ to $\{h = h_{LK}(0)\}$ under the flow of (9).

Next, we consider how the durations of various phases change as g_{app_1} is increased. We will explain why the silent and active phases of both cells become shorter, but not much shorter, for our biologically relevant parameter set, as seen in Figure 7. As in Section 3.1, we list several properties of the v–nullcline, including some effects on the v–nullcline achieved by varying g_{app}. The postinhibitory rebound case differs from the persistent sodium case in that the persistent sodium current $I_{NaP} = g_{NaP} m_\infty(v) h(v - e_{Na})$ is replaced by a T–type calcium current $I_T = g_T m_\infty(v) h(v - v_{Ca})$. Therefore, analogously to Section 3.1, we have $\partial F/\partial h = -g_T m_\infty(v_L)(v_L - v_{ca})$ with small $m_\infty(v)$ over the silent phase, and the following conditions hold:

($E1$) An increase in g_{app_1} causes the v–nullcline for cell 1 to shift to a lower h value for each fixed $v < 0$, and to a higher h value for each fixed $v > 0$, with

$$\partial v_L(h, s, g_{app})/\partial g_{app} > 0. \tag{20}$$

The size of the shift in the v-nullcline is proportional to v, such that $\partial v_R(h, g_{app})/\partial g_{app}$

is quite small for all relevant h.

$(E2)$ Large shifts in the v-nullcline in the h direction due to changes in g_{app} are translated into smaller changes in v_L.

$(E3)$ Based on calculations analogous to the derivation of (19) and the small size of $(-v_{RK})/g_T m_\infty(v_{RK})(v_{RK} - v_{na})$ for each $v_{RK}(0, g_{app})$, the h-coordinate of the left knee decreases significantly as g_{app} increases, while the h-coordinate of the right knee changes negligibly.

We also append one additional hypothesis to this list of properties, since this arises for the parameter regime that we consider.

$(H3)$ The fixed points lie on the steep part of the h–nullcline.

Assuming $(H1) - (H2)$, effects $(E1) - (E3)$ follow, and we also assume $(H3)$. Let $h_1(t)$ denote the h–coordinate of cell 1 along the balanced half-center oscillation described in section 2.4.2, with $h_1(0) = h_{RK}(0)$. Suppose that in the asymmetric case, at time $t = 0$, the h-coordinate of cell 1 lies at $h_{RK}(0)$ as well, and let $\hat{h}_1(t)$ denote the h-coordinate of cell 1 in the ensuing solution, also assuming, as stated above, that at time 0, cell 2 lies at $(v_L(h_1(s_{max}), s_{max}), h_1(s_{max}))$. Cell 1 jumps down when it reaches $\{h = \hat{h}_{RK}(0)\}$, which occurs almost immediately since $(E3)$ implies $\hat{h}_{RK}(0) \approx h_{RK}(0)$. The location of cell 2 implies that it jumps up instantly in response to the associated release from inhibition. In the silent phase, we have $\hat{h}_1(t) < h_1(t)$ due to $(E1)$. Because cell 2 receives no extra drive, it jumps down after essentially the same active phase duration T_A present in the balanced case, with $\hat{h}_1(T_A) < h_1(T_A)$. Thus, cell 1 enters the active phase at a smaller h than in the balanced case. Cell 1 jumps down from the active phase when $\hat{h}_1 = \hat{h}_{RK}(0)$. As noted above, $(E3)$ implies that $\hat{h}_{RK}(0) \approx h_{RK}(0)$. Hence, the active phase duration $\hat{T}_A^1$ satisfies $\hat{T}_A^1 < T_A$. As a result, cell 2 jumps down from a smaller h value than in the balanced case. Repeating the above arguments yields a sequence of successively shorter silent phase durations for each cell. Moreover, both sequences must converge, if the existence conditions for a half-center oscillation are satisfied.

Now, we have established that the durations of all phases of the oscillation become shorter when extra drive is applied to one cell in the postinhibitory rebound case. We now explain why these changes are, in fact, quite small (e.g., see Figure 7B). The changes observed are all linked to the fact that, given the same starting h–coordinate in the silent phase, a cell receiving extra drive reaches a smaller h before release from inhibition than a cell receiving baseline drive. There are four possible effects that could squelch this difference, and three of them are observed for our system. The first possibility is that the fixed point in the silent phase lies at similar h–values as g_{app} varies and jump up occurs near the fixed point. But this is not observed here, by $(H3)$; indeed, $(H3)$ helps ensure that the changes in phase durations are non-negligible. Given that the fixed points are at quite different values, the second and third possible effects both follow from the fact that the rate of change of h is sufficiently faster in the active phase than in the silent phase. This difference means that the cells jump up from positions far below their respective fixed points, before they have time to spread out substantially. It also implies that differences in h at jump up translate into very small differences in time spent in the following active phase. We observe both of these effects (see Figure 7). Finally, $(E2)$ helps bound the differences in rate of change of h in the silent phase between the cells with and without extra drive, although this is not a strong factor for our postinhibitory rebound model.

3.3 Half-center CPG based on neuronal adaptation

For the balanced half-center oscillator based on adaptation, phase transitions occur when the inhibition to the cell in the silent phase has decreased enough so that the cell reaches the appropriate left knee and jumps up to the active phase, inhibiting the cell that is already there. For the balanced case $g_{app_1} = g_{app_2}$, the conditions (15),(16) suffice to give the existence of a stable half-center oscillation. These conditions ensure that the cell in the silent phase is able to reach the curve of left knees $p_{LK}(s)$ and that when the active cell becomes inhibited, it immediately jumps down to the silent phase. As in subsection 2.4.3, we focus on Case 1. This choice is motivated by the fact that

the Case 1 model is more similar to the persistent sodium model than is Case 2. Hence, the differences between Case 1 and persistent sodium that we illustrate will be even stronger between Case 2 and persistent sodium (see Table 1), by completely analogous arguments.

As shown in Figure 1C, once $g_{app_1} > g_{app_2}$, there are four nullclines to consider for the pair of coupled cells. If g_{app_1} is not increased too much, then both cells have critical points in the silent phase in the absence of coupling, and the phase switches still occur when each cell reaches its left knee and jumps up. The shifts in the nullclines yield a new value $\hat{\sigma}$ where the fixed point curve meets the curve of left knees for the cell with extra drive and new intervals $\hat{I}_L, \hat{I}_R$ analogous to I_L, I_R in subsection 2.4.3 and Figure 2; see Figure 8. In the case with $g_{app_1} > g_{app_2}$, establishing the existence of a singular periodic solution requires that both of the jumping conditions are met both when cell 1 is silent and cell 2 is active and vice versa. The arguments in subsection 2.4.3 generalize immediately to imply that the solution exists if two pairs of conditions are met. The first pair of conditions are

$$\sigma > \hat{s}(\widehat{Ca}_{RK}(s_{max})), \text{ and } \hat{\sigma} > s(Ca_{RK}(s_{max})),$$

where σ ($\hat{\sigma}$) is the s value at which the curves of fixed points and left knees intersect for baseline (extra) drive, as in subsection 2.4.3 and $s(Ca)$, $\hat{s}(\widehat{Ca})$ are given by evaluating equation (13) at $v_R(Ca, 0)$ and $\hat{v}_R(\widehat{Ca}, 0)$, respectively. The second pair of conditions are

$$\hat{T}_A(Ca) < T_S(Ca), \forall Ca \in \hat{I}_L, \text{ and } T_A(Ca) < \hat{T}_S(Ca), \forall Ca \in I_L,$$

where $\hat{T}$ terms denote evolution times for the cell with extra drive.

Next, we consider how the durations of various phases change as g_{app_1} is increased. As in Sections 3.1 and 3.2 we want to understand how changes in g_{app_1} affect the v–nullcline. Analogously to the previous sections, we catalog a set of effects that g_{app} has on the v–nullcline. To do this, we now write $dv/dt = F(v, Ca, s, g_{app})$, to make explicit the role of g_{app}. Similarly, the branches of the v–nullcline can be expressed as $v_X(Ca, s, g_{app})$ and $\hat{v}_X(Ca, s, g_{app})$ for $X \in \{L, M, R\}$, depending on the level of drive.

($E1$) An increase in g_{app_1} causes the v-nullcline for cell 1 to shift to a higher Ca value for each fixed $v < 0$, and to a lower Ca value for each fixed $v > 0$. The size of the shift is proportional to $v - v_{app} = v$. Thus, the greatest effects of the increase appear in the silent phase, where $\partial v_L(Ca, s, g_{app})/\partial g_{app} > 0$.

($E2$) Large shifts in the v–nullcline in the Ca direction due to changes in g_{app} are translated into smaller changes in v.

($E3$) The Ca–coordinate of the left knee increases significantly as g_{app} increases.

We append four additional hypotheses to this list of effects.

($H3$) The Ca–nullcline intersects the inhibited v–nullclines on their left branches $v_L(Ca, s, g_{app})$ for s sufficiently large. Therefore, the cell in the silent phase is not able the reach the left knee when it is maximally inhibited, and phase switching depends on there being some decay of synaptic strength, due to the evolution of the cell in the active phase. Note that despite this second intersection, we use $(v_{FP}, Ca_{FP}), (\hat{v}_{FP}, \hat{Ca}_{FP})$ to denote the fixed point on the right branch of the uninhibited nullcline for the baseline and extra drive cases, respectively.

($H4$) $|\partial Ca_{LK}/\partial s|$ is sufficiently large.

($H5$) Adaptation of the active cell becomes significant only near its fixed points (i.e., θ_s in equation (2) is near v_{FP}).

($H6$) The fixed points satisfy $v_{FP} < v_{app}$, and the Ca–nullcline is not too steep where they occur.

Below, we clarify what is meant by ($H4$) and ($H6$).

Assuming $(H1) - (H2)$, effects $(E1) - (E3)$ follow. We now deduce the temporal effects of changing g_{app_1}. Qualitatively, the cells still follow trajectories in the (Ca, s) plane that are similar to those in Figure 2A, although the relevant range of Ca for cell 1 shifts as discussed above. Assume that at time 0, cell 2 lies at its jump up point from the balanced case, $(v_{LK}(s), Ca_{LK}(s))$ for some $s \in (0, s_{max})$, and cell 1 lies at its jump

down point from the balanced case, with $\widehat{Ca}_1 \in I_R$. Cell 2 jumps up and evolves under equation (10) along the same path it followed in the balanced case until cell 1 jumps up again. We consider how long it takes for this to occur, relative to the balanced silent phase duration T_S. By $(E1)$, and the form of the equations in system (5), Ca_1 evolves more slowly than in the balanced case, following a different path in (Ca_1, s_2)-space as s_2 decays, which is necessary by $(H3)$. On the other hand, by $(E3)$, the curve of left knees lies at larger Ca_1 for cell 1 than in the balanced case; that is, $\widehat{Ca}_{LK} > Ca_{LK}$ for each s. The key question is, does s_2 decay more or less than in the balanced case by the time cell 1 hits the curve of knees?

The answer depends on how $\dot{Ca}$ and Ca_{LK} change with g_{app} as well as on $|\partial Ca_{LK}/\partial s|$, as illustrated in Figure 8 A and B. If $\dot{Ca}$ depends strongly on g_{app}, then this promotes a long silent phase (dotted curves in Figure 8). However, this case is not what we observe, by $(E2)$. On the other hand, $(E3)$ implies that Ca_{LK} increases significantly with g_{app}, which prevents the silent phase from becoming too long and could potentially even shorten it. Finally, a large $|\partial Ca_{LK}/\partial s|$, as assumed in $(H4)$, also promotes a shorter silent phase, as shown in Figure 8. In sum, while the effect is weak due to the slower evolution of Ca_1 in the silent phase relative to the balanced case, Ca_1 at jump-up will be larger in the asymmetric case, and the silent phase $\hat{T}_S^1$ will be shorter than T_S under $(H1) - (H4)$; see Figure 8B. We next show that cell 1 jumps down at similar Ca in both cases, such that these arguments persist beyond the first oscillation cycle.

To do this, we continue to follow cell 1 beyond its jump up to the active phase. As we just showed, the jump up occurs at a larger Ca than in the balanced case, which could promote a shorter active phase. By $(H3)$, however, the cell in the active phase must reach a sufficiently large Ca for adaptation to become significant and release the silent cell. Moreover, by $(H5)$, this release requires the active cell in each case to reach a small neighborhood of its fixed point, which compresses the difference in Ca. Finally, a key point is that by $(H6)$, $\widehat{Ca}_{FP} > Ca_{FP}$ and $\hat{v}_{FP} > v_{FP}$. The latter inequality implies that s_1 will adapt more slowly in the asymmetric case than in the balanced case, causing cell 2 to spend a *longer* time in the silent phase. If the Ca–nullcline were very steep at

the fixed point, then the difference $\hat{v}_{FP} - v_{FP}$ would be very small in magnitude. Under $(H6)$, this difference is more significant, although it may still be quantitatively small, ensuring that this is the dominant effect in determining the phase duration. Moreover, (H6) also implies that $\hat{Ca}_{FP} - Ca_{FP}$ is small and hence cell 1 jumps down from a similar Ca–value in both cases, as claimed.

Figure 9 illustrates the adaptation case with increased g_{app_1} when $(H1) - (H6)$, and hence $(E1) - (E3)$, hold. The jump down point of the reference orbit (balanced case, black) is close to the critical point. Figure 9 shows that the duration of the silent phase of cell 1 and therefore the active phase of cell 2 is shorter compared to the asymmetric case. The duration of the active phase of cell 1 and therefore the duration of the silent phase of cell 2 is prolonged.

3.4 Slow synaptic decay

In the previous sections, we analyzed the effect of increasing g_{app_1} when synaptic decay occurs on the fast timescale. Our results carry over directly when synaptic decay occurs on the slow timescale. Slow synaptic decay is modelled by assuming $\beta = O(\epsilon)$ in systems (3) and (4). This assumption implies that $s_{max} = 1$ in the singular limit, but we will continue to refer to s_{max} for consistency with previous sections.

Figure 15 illustrates the changes in silent phase durations for cell 1 and 2 for several increased values of g_{app_1} in the model systems that we consider, with slow synaptic decay. The results are qualitatively identical to those in Figure 5. In some cases, the effect of changing g_{app} is quantitatively weaker when the synaptic decay is slow, and the range of g_{app_1}/g_{app_2} over which half-center oscillations exist may be reduced. In Figures 11A, 12A, 14A, the baseline drive nullclines and the extra drive nullclines are closer together than in the fast synaptic decay cases due to correspondingly smaller choices of g_{app}.

The mechanisms that contribute to the observed changes in phase durations are similar across synaptic decay rates. The analysis, however, becomes more complicated

when synapses decay slowly. The simplest aspect to analyze is the existence of a periodic singular bursting solution with $g_{app_1} = g_{app_2}$ in the persistent sodium model, which we consider here. Suppose cell 1 starts at $(v_R(h_1(0), 0), h_1(0))$, with $h_1(0) \in [h_{FP}(0), h_{RK}(s_{max})]$ and cell 2 starts at $(v_{LK}(s_{max}), h_{LK}(s_{max}))$; see Figure 10A. Cell 2 jumps up to the right branch of the inhibited v–nullcline, to $(v_R(h_{LK}(s_{max}), s_{max}), h_{LK}(s_{max}))$. Cell 1 is inhibited by cell 2 and jumps down to the silent phase, because $h_1(0) \in [h_{FP}(0), h_{RK}(s_{max})]$. While cell 2 evolves in the active phase, the inhibition to cell 2 slowly decays to a value, say ρ, during the time, say T_d, that cell 1 needs to reach the left knee and jump up into the active phase. Cell 2 is able to jump down to the silent phase if the inhibition decays fast enough so that its corresponding h–value, $h_1(\rho)$, lies in the interval $[h_{FP}(\sigma), h_{RK}(s_{max})]$. Figure 10B illustrates the decay of inhibition to cell 2 in the slow phase plane.

Although there are two slow variables in the active phase, both cells always jump up with $h = h_{LK}(s_{max})$ and $s = s_{max}$. Thus, the cells always enter the active phase with the same initial conditions and correspondingly follow the same 1-d trajectory $(h(t), s(t) = s_{max}e^{-\beta t})$ in the active phase. Since this trajectory is monotone in both components, we can express $s = s(h)$ along it. The shortest possible time that a cell will spend in the silent phase is $T_S(h_{RK}(s_{max}))$, the time of evolution of h from $h_{RK}(s_{max})$ to $h_{LK}(s_{max})$ under the flow of (9). Analogously to the previous sections, the existence of a periodic singular solution is guaranteed if

$$T_A(h_{RK}(s_{max})) < T_S(h_{RK}(s_{max})),$$

where the former is the evolution time from $(h_{LK}(s_{max}), s_{max})$ to $(h_{RK}(s_{max}), s(h_{RK}(s_{max}))$ under the flow of

$$\begin{aligned} \dot{h} &= g(v_R(h, s), h), \\ \dot{s} &= -\beta s. \end{aligned}$$

The above analysis shows that because the dynamics of the decay of s is independent of the evolution of h and the phase transition is governed by the cell in the silent phase, the slow decay of s has minimal impact on the half-center oscillation. Indeed, although we omit the details, the same factors as discussed in subsection 3.1 yield a shorter silent

phase of cell 1 and only a negligible change in the silent phase duration of cell 2 when $g_{app_1} > g_{app_2}$, as shown in Figure 11.

Analysis with slow synaptic decay in the other models is more complicated. In the adaptation model, recall from subsection 3.3 that the jump up required crossing a curve of left knees, parameterized by s, in the silent phase. Slow synaptic decay introduces slow dynamics of s, which imply that the level of s is no longer strictly slaved to the voltage of the active cell. Slow synaptic decay continues in the active phase as well, introducing continuous variation of the position of the nullcline on which each cell evolves when active, but this is a more minor effect since s only weakly affects nullcline position in the active phase; see Figure 12.

In the postinhibitory rebound case, the slow decay of inhibition also influences how cells jump up from the silent phase, as shown in Figure 13. Moreover, as with adaptation, the decay of inhibition continues to be a factor while each cell is active. The existence of a periodic half-center oscillation in the balanced case with slow synaptic decay can be analyzed using a map approach as in previous sections, and in fact similar analysis has been done previously (e.g., Rubin and Terman, 2000). Introducing extra drive, with $g_{app_1} > g_{app_2}$, complicates the precise arguments, but again, the relevant mechanisms remain those discussed in subsection 3.2, and the effects on oscillation period are qualitatively similar to those observed with fast decay; see Figure 14.

4 Discussion

We have considered the generation of oscillations in three reduced half-center CPG models encapsulating three different dynamic mechanisms for phase transitions, embodied through persistent sodium current, postinhibitory rebound, and a calcium-dependent adaptation, respectively, together with mutual synaptic inhibition. By considering asymmetric drives, we have uncovered a critical distinction between adaptability of CPGs composed of units with different types of intrinsic dynamics, in contrast with the emphasis of previous studies. The mathematical analysis that we have given provides a specific accounting of the factors in the phase plane dynamics corresponding to each

model that determine its responses to variations in drive, and how each factor contributes. The generality of this analysis ensures that any parameter set that maintains qualitatively similar dynamical features will yield similar outcomes, while more substantial parameter variations may change the dynamic structure of a model and alter the effects of drive modulation correspondingly.

As summarized in Tables 1-3, our results show that oscillations based on the postinhibitory rebound model or on adaptation in Case 2, where an increase in drive conductance g_{app} can yield an increase in period, share common traits. In particular, both show high stability, with half-center oscillations maintained over a large range of g_{app} and over a large ratio of g_{app_1}/g_{app_2}. At the same time, both mechanisms, and particularly postinhibitory rebound, yield insensitivity of period to g_{app} and an inability to tune phase durations independently via asymmetric drive, which would limit their effectiveness within a feedback loop. In contrast, oscillations based on persistent sodium exhibit the greatest sensitivity of period to g_{app} and achieve the largest range of periods, although they persist over a relatively small range of g_{app}. Moreover, with asymmetric drive, persistent sodium-based oscillations show the greatest range of phase durations and the highest independence in phase duration control.

At first glance, the CPG models based on persistent sodium current and postinhibitory rebound may appear to be mirror images of each other, with one cell clearly in control of each switch between phases. However, the scaling of the effects of inhibitory coupling, and of excitatory drive, with postsynaptic potential breaks the symmetry between these models and causes them to respond differently to drive modulation. In fact, the models based on persistent sodium current and on adaptation are arguably more closely related to each other and less similar to postinhibitory rebound. In the model based on postinhibitory rebound, transitions occur when the active cell falls down from the active phase, releasing the suppressed cell from inhibition [29]. In both of the other models, transitions occur when the silent cell reaches a knee or curve of knees from which it can escape from the silent phase, and this escape yields inhibition of the active cell, terminating its activity. In the model based on adaptation, however, escape

cannot occur unless it is accompanied by a partial synaptic release due to adaptation. Indeed, it is appropriate to think of the models based on persistent sodium current and adaptation as points on a continuum. The persistent sodium-based model lies in an extreme position, with little or no change in the strength of the synaptic output from a cell while it is active. Moving along the continuum away from this extreme, by increasing the synaptic threshold for example, yields progressively more adaptation, or weakening of synaptic output during the latter stages of the active phase. Our Case 2 of adaptation represents a point along this continuum that is farther away from the persistent sodium model than is our Case 1, yielding a non-monotonic dependence of period on drive in the balanced drive regime, as observed by other authors [27, 30]. The more extreme nature of Case 2 is also reflected in the stronger changes observed with asymmetric drives. More generally, different susceptibilities to drive modulation and different degrees of independent phase control would arise at different points along the continuum, interpolating between the cases that we have considered.

As noted in the Introduction, the specific intrinsic neural mechanisms involved in the generation of locomotor oscillations in most CPGs, especially in mammals, remain largely unknown. What is known is that these CPGs are extremely flexible and can adaptively adjust the oscillatory patterns they generate to the motor demands they face. This flexibility includes the ability to generate oscillations with a wide range of frequencies, combined with independent regulation of each phase duration under the control of descending drives, even in the absence of phasic afferent feedback (e.g., as seen in fictive locomotion, [17],[38]). If we assume that the structure and operation of at least some biological CPGs (e.g., the spinal locomotor CPG) can, in a simplified sense, be represented by half-center models, then it is important to elucidate what dynamic mechanisms could potentially provide this flexibility. Since the precise features involved in the operation of most CPGs are unknown, we felt that it was reasonable to comparatively investigate different half-center models, incorporating different intrinsic dynamic mechanisms, with a particular focus on how different components yield different responses to changes in drive. In particular, previous numerical simulations [25]

have demonstrated that a half-center model of the spinal CPG based on the dynamics of the persistent sodium current can reproduce the full range of locomotor periods and phase durations observed during fictive and treadmill locomotion in cats. This computational model, however, has not been theoretically investigated in detail, and CPG models based on other intrinsic mechanisms have not been previously studied in the context considered here, namely their operation in regimes of asymmetric drive. Here we have shown that the persistent sodium current-based half-center CPG model achieves a greater range of oscillation periods with changes in the drives to both half-centers than other typical half-center models considered. Moreover, this model provides a unique possibility for the independent control of each phase duration in the asymmetric regime attained by changing drive to only one half-center. These findings provide additional support for the possibly important role of persistent sodium current-dependent mechanisms in the operation of biological CPGs, and especially in the operation of the spinal locomotor CPG.

One set of previous studies that have considered frequency control and asymmetry within a half-center CPG system has made use of dynamic clamp technology to generate hybrid systems composed of a biological neuron synaptically coupled to a simulated neuron [33],[19]. In particular, it was recognized that independent phase regulation could be achieved by modulation of the time constant of a slow current or the conductance of a particular ionic current, in one cell within a half-center system with an adaptation-type phase transition mechanism [19]. We have considered a more direct form of modulation, namely variation of the external drive to one cell, rather than its internal parameters. Nonetheless, given the ubiquity of neuromodulators in neuronal systems, it is likely that multiple modulatory mechanisms exist, which together enable control of oscillatory properties through effects on multiple targets.

Our analysis focused on reduced models, with each cell's intrinsic dynamics represented in a two-dimensional phase plane. Such reductions are known to capture fundamental effects present in higher-dimensional models (e.g., [22],[23],[24],[29],[32]) while allowing for analytical tractability. Unlike previous reduced models for CPGs

and other rhythmic systems based on firing rate formalisms [16],[27],[34],[35], the reduced models we consider are conductance-based, such that transition mechanisms and model parameters are connected directly to particular biological features. Nonetheless, future theoretical studies should examine how the results observed here are affected by the presence of additional currents observed in specific biological CPGs, as well as synaptic effects such as short-term synaptic plasticity [34],[35], and how these results scale up to larger networks incorporating biologically relevant connectivity architectures and neuromodulatory pathways. Such extensions will elucidate further details about the mechanisms through which particular CPG units subserve different behaviors.

Acknowledgments S. Daun received support from NIH grant R01 HL76137. J.E. Rubin received support from NSF award DMS 0716936. I.A. Rybak was supported by NIH grants RO1 NS048844 and RO1 NS057815.

5 Appendix

Here, we list the auxiliary functions and parameter values used in the three example systems that we consider, as introduced in Section 2.2.

5.1 Model featuring the persistent sodium current [3]

The ordinary differential equations for the model featuring the persistent sodium current are

$$\begin{aligned} C_m v' &= -I_{NaP} - I_L - I_{syn} - I_{app}, \\ h' &= (h_\infty(v) - h)/\tau_h(v), \\ s' &= \alpha(1-s)s_\infty(v) - \beta s, \end{aligned} \tag{21}$$

with associated functions

$$I_{syn} = g_{syn} s (v - e_{syn}),$$

$$
\begin{aligned}
I_{NaP} &= g_{nap} m_\infty(v) h(v - e_{na}), \\
I_L &= g_l(v - e_l), \\
I_{app} &= g_{app} v, \\
h_\infty(v) &= 1/(1 + \exp((v - \theta_h)/\sigma_h)), \\
s_\infty(v) &= 1/(1 + \exp((v - \theta_{syn})/\sigma_{syn})), \\
\tau_h(v) &= \epsilon \cosh((v - \theta_h)/\sigma_h/2), \text{ and} \\
m_\infty(v) &= 1/(1 + \exp((v - \theta_m)/\sigma_m)),
\end{aligned}
$$

where $C_m = 0.21$, $g_{nap} = 10$, $g_l = 2.8$, $e_{na} = 50$, $e_l = -65$, $e_{syn} = -80$, $\theta_m = -37$, $\sigma_m = -6$, $\theta_h = -30$, $\sigma_h = 6$, $\epsilon = 0.01$, $\theta_{syn} = -43$, $\sigma_{syn} = -0.1$, $g_{syn} = 1$, $g_{app} = 0.19$, $\alpha = 1$, and $\beta = 1$ (fast decay) or $\beta = 0.08$ (slow decay).

5.2 Model featuring postinhibitory rebound [24, 31]

For the model featuring postinhibitory rebound, the relevant differential equations are

$$
\begin{aligned}
C_m v' &= -I_T - I_L - I_{syn} - I_{app}, \\
h' &= (h_\infty(v) - h)/\tau_h(v), \\
s' &= \alpha(1 - s) s_\infty(v) - \beta s,
\end{aligned}
$$

with associated functions

$$
\begin{aligned}
I_{syn} &= g_{syn} s(v - e_{syn}), \qquad (22) \\
I_{app} &= g_{app} v, \\
I_L &= g_l(v - v_l), \\
I_T &= g_T m_\infty(v) h(v - v_{ca}), \\
m_\infty(v) &= 1/(1 + \exp(-(v - \theta_m)/\sigma_m)), \\
h_\infty(v) &= 1/(1 + \exp(-(v - \theta_h)/\sigma_h)), \\
\tau_h(v) &= t_0 + t_1/(1 + \exp(-(v - \theta_{ht})/\sigma_{ht})), \text{ and}
\end{aligned}
$$

$$s_\infty(v) \;=\; 1/(1+\exp((v-\theta_{syn})/\sigma_{syn})),$$

where $g_T = 4$, $v_{ca} = 90$, $\theta_m = -40$, $\sigma_m = 7.4$, $\theta_h = -70$, $\sigma_h = -4$, $\theta_{ht} = -50$, $\sigma_{ht} = -3$, $g_l = 0.4$, $v_l = -70$, $t_0 = 30$, $t_1 = 200$, $g_{syn} = 1.4$, $v_{syn} = -85$, $\theta_{syn} = -35$, $\sigma_{syn} = -0.1$, $g_{app} = 0.01$, $\alpha = 1$, and $\beta = 1$ (fast decay) or $\beta = 0.05$ (slow decay).

5.3 Model featuring adaptation (modified from [9])

The model featuring adaptation is given by the differential equations

$$\begin{aligned} C_m v' &= -I_{Ca} - I_{ahp} - I_L - I_{syn} - I_{app}, \\ Ca' &= \epsilon(-g_{ca} I_{Ca}(v) - k_{ca}(Ca - ca_{base})), \\ s' &= ((1-s)s_\infty(v) - ks)/\tau_s, \end{aligned}$$

with associated functions

$$\begin{aligned} m_\infty(v) &= 1/(1+\exp((v-\theta_m)/\sigma_m)), \\ s_\infty(v) &= 1/(1+\exp((v-\theta_{syn})/\sigma_{syn})), \\ Ca_\infty(v) &= 1/(1+\exp((v-\theta_{ca})/\sigma_{ca})), \\ I_L &= g_l(v-e_l), \\ I_{app} &= g_{app} v, \\ I_{syn} &= g_{syn} s(v-e_{syn}), \\ I_{ahp} &= g_{ahp}(v-e_k)(Ca^2)/(Ca^2 + k_{ahp}^2), \text{ and} \\ I_{ca} &= \bar{g}_{ca}((Ca_\infty(v))^2)(v-v_{ca}). \end{aligned} \tag{23}$$

In Case 1, $C_m = 21$, $g_{syn} = 2$, $g_{app} = 0.7$, $e_l = -55$, $\theta_m = -34$, $\sigma_m = -5$, $e_k = -85$, $g_l = 1$, $e_{syn} = -70$, $k = 1$, $\tau_s = 1$ (fast decay) or $\tau_s = 400$ (slow decay), $\sigma_{syn} = -5$, $\theta_{syn} = -20$, $\theta_{ca} = -34$, $\sigma_{ca} = -8.0$, $k_{ca} = 22.5$, $\epsilon = 5e-05$, $k_{ahp} = 0.7$, $v_{ca} = 140$, $g_{ahp} = 7$, $g_{ca} = 0.05$, $g_{ca1} = 1$, and $ca_{base} = 0.08$. In Case 2, the same parameters are

used except $g_{syn} = 6$ (fast decay) or $g_{syn} = 4$ (slow decay), $e_{syn} = 50, k = 0.02$ (fast decay) or $k = 0.002$ (slow decay), $\sigma_{syn} = -4$, and $\theta_{syn} = 20$.

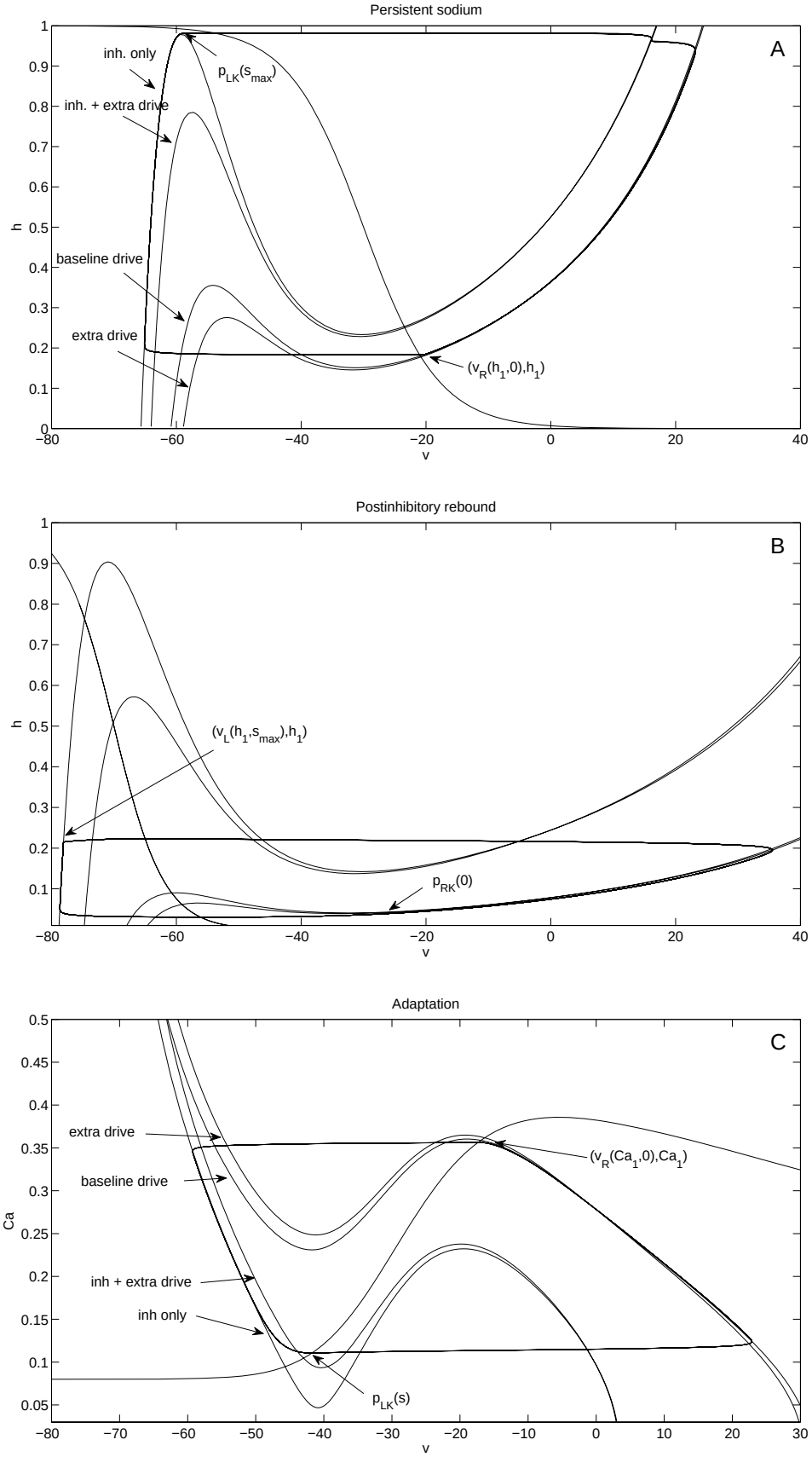

Figure 1: *Basic nullcline configurations and periodic orbits for the three half-center oscillation mechanisms (see sections 2.2 and 2.4). Half-center oscillations based on (A) persistent sodium, (B) postinhibitory rebound, and (C) adaptation. Note that inh denotes inhibition, while other notation is defined in the text.*

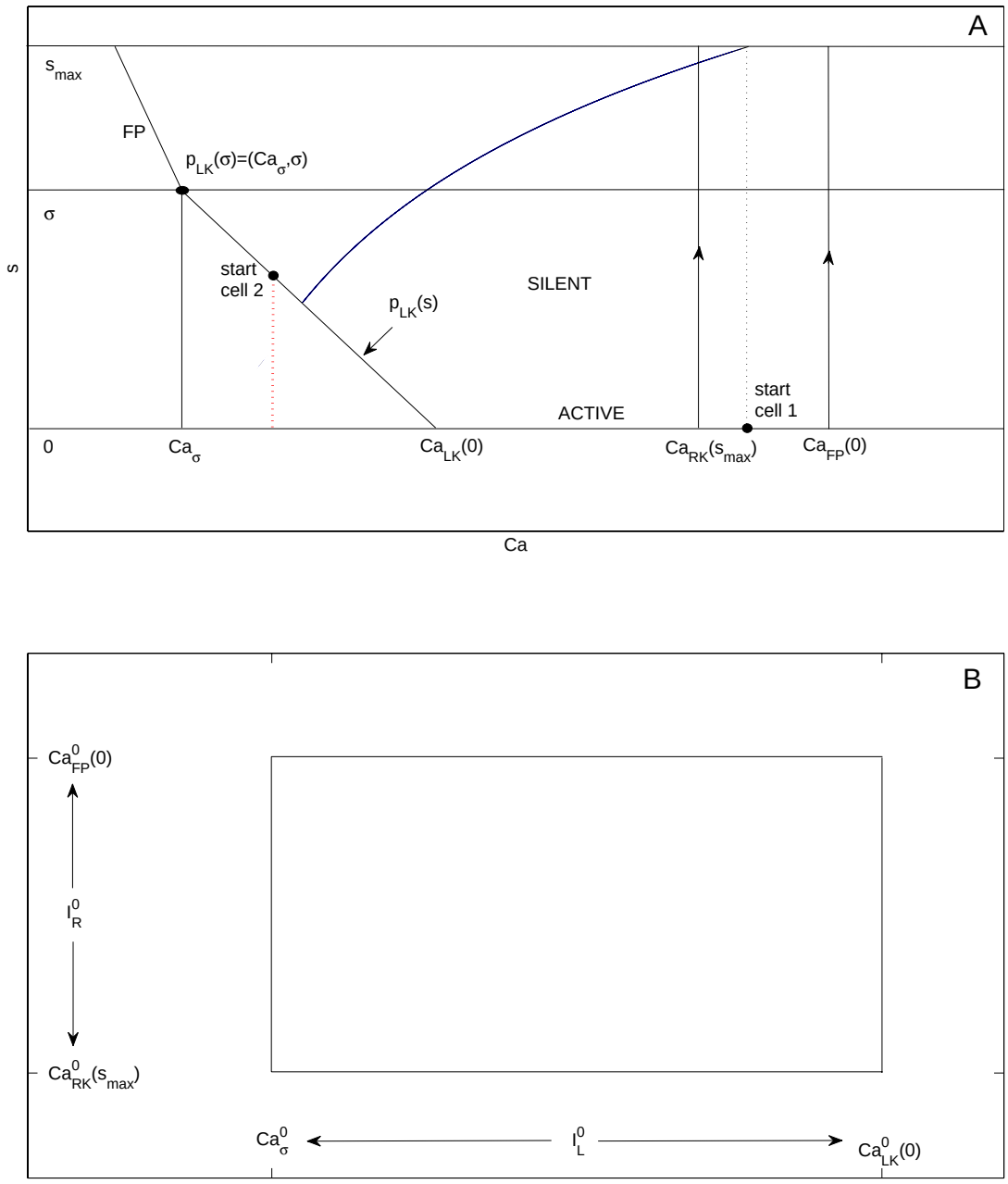

Figure 2: *Existence of a periodic oscillation for the adaptation model can be established using a contraction argument. (A) (Ca, s) phase plane. When a cell is in the active phase, it evolves along $\{s = 0\}$. When a cell is in the silent phase, it evolves in the region with $s > 0$, with the decay rate of s determined by the position of the other cell in the active phase. The vertical dotted lines indicate that, for the starting configurations shown, cells 1 and 2 switch phases immediately. (B) The rectangle R_{Ca}. The existence of a periodic oscillation is guaranteed if for all $(Ca_2, Ca_1) \in R_{Ca}$, $(\tilde{Ca}_2, \tilde{Ca}_1) \in int(R_{Ca})$.*

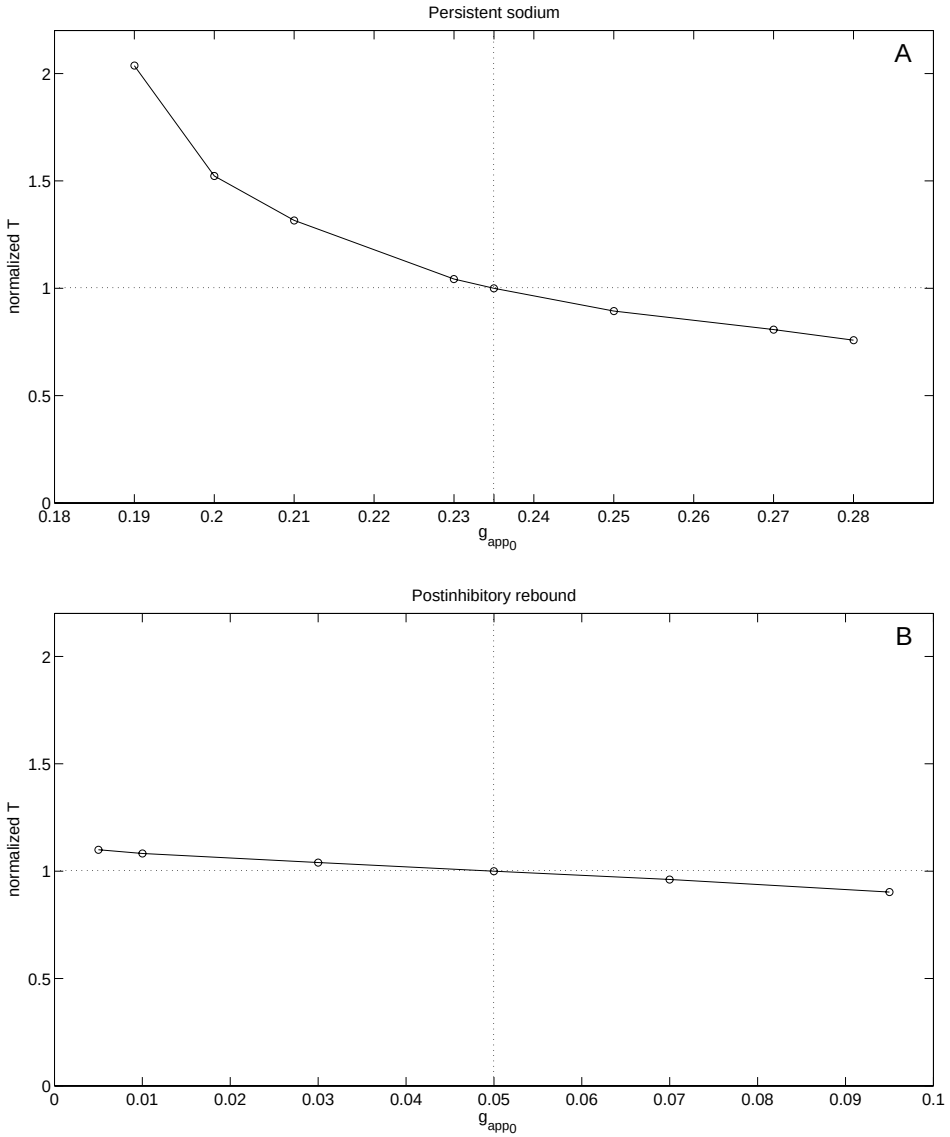
Persistent sodium
A
normalized T
2
1.5
1
0.5
0
0.18
0.19
0.2
0.21
0.22
0.23
0.24
0.25
0.26
0.27
0.28
g_{app_0}
Postinhibitory rebound
B
normalized T
2
1.5
1
0.5
0
0
0.01
0.02
0.03
0.04
0.05
0.06
0.07
0.08
0.09
0.1
g_{app_0}

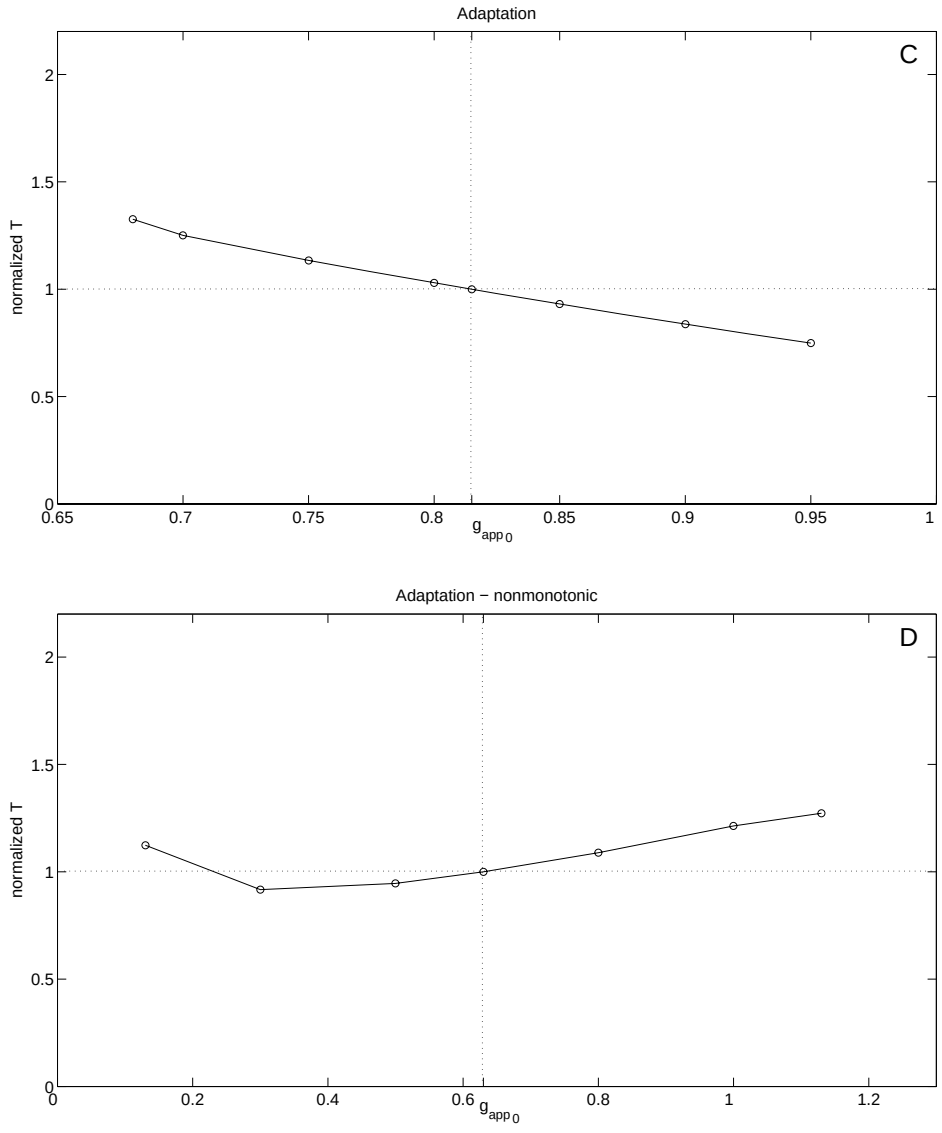

Figure 3: *The periods of the basic periodic orbits shown in Figure 1 change with changes in drive to both cells. Half-center oscillations based on (A) persistent sodium, (B) postinhibitory rebound, (C) adaptation, Case 1, (D) adaptation, Case 2.*

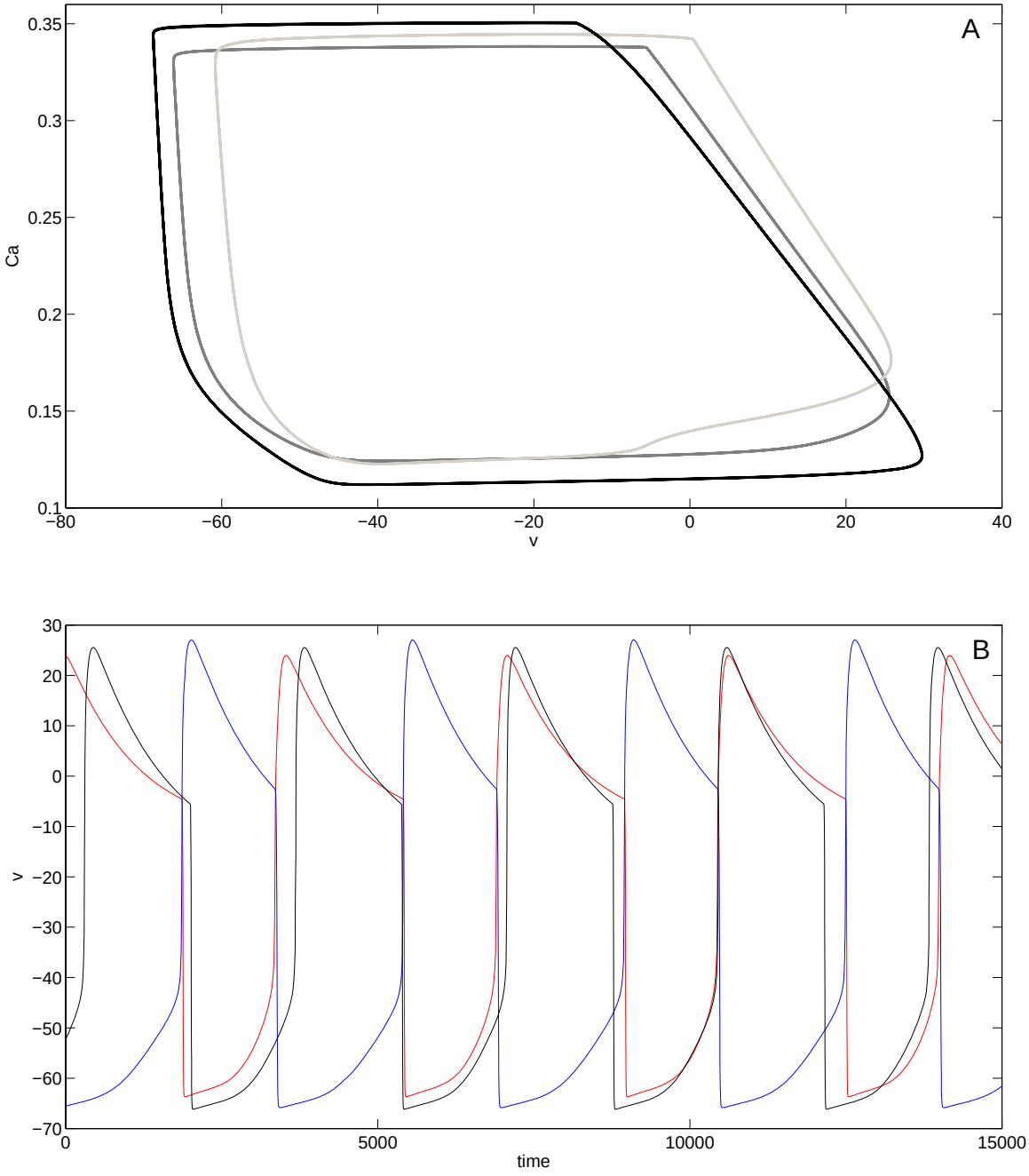

Figure 4: *Periodic oscillations in Case 2 of the adaptation model. (A) Periodic orbits for* $g_{app_1} = g_{app_2} = 0.13$ *(black),* $g_{app_1} = g_{app_2} = 0.3$ *(dark grey),* $g_{app_1} = g_{app_2} = 0.7$ *(light grey), with balanced drive. (B) Time courses for periodic oscillations in the balanced (black) and asymmetric (cell 1 (red), with increased drive, and cell 2 (blue)) cases.*

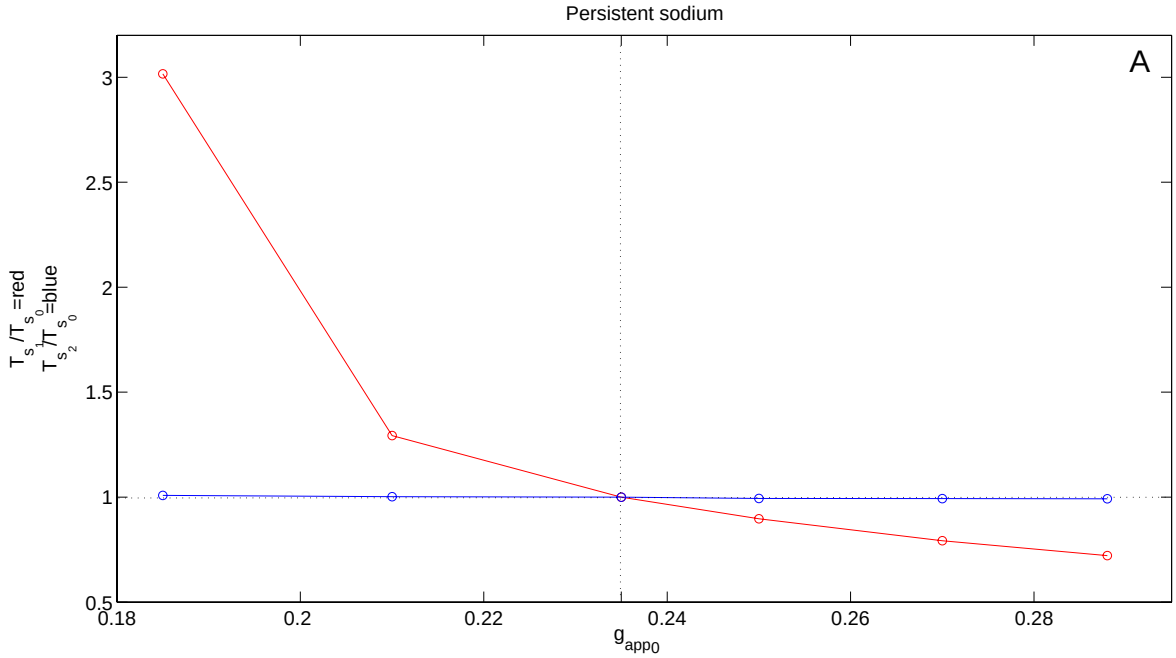
Persistent sodium
A
3
2.5
2
1.5
1
0.5
0.18
0.2
0.22
0.24
0.26
0.28
g_{app0}
T_{s_1}/T_{s_0}=red
T_{s_2}/T_{s_0}=blue

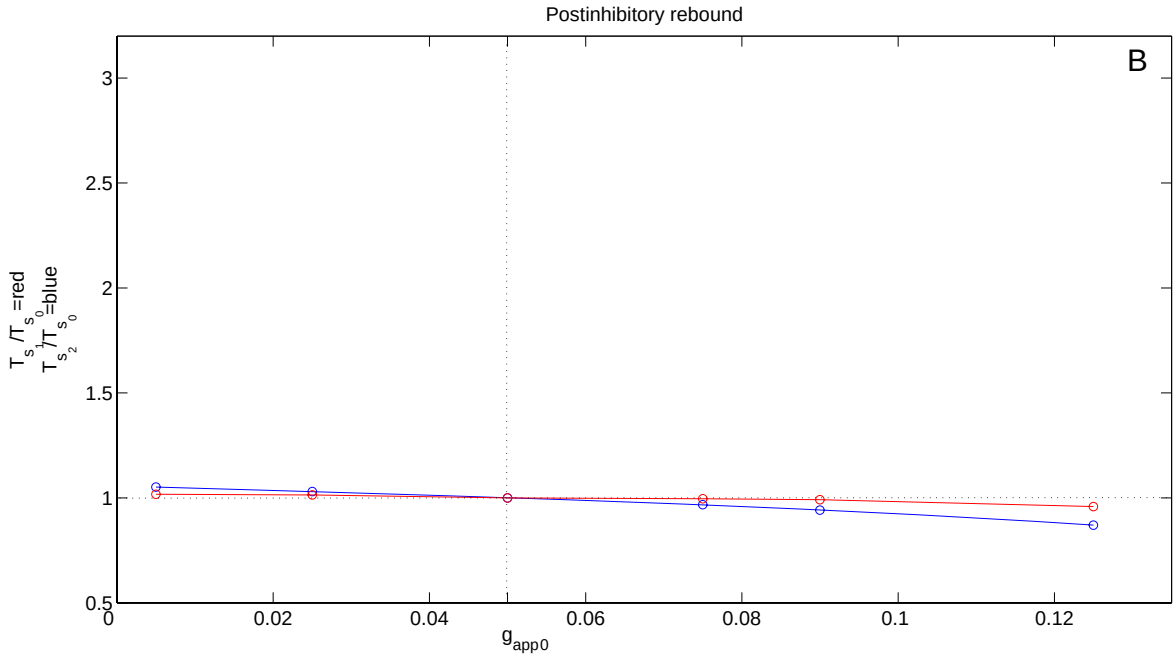
Postinhibitory rebound
B
3
2.5
2
1.5
1
0.5
0
0.02
0.04
0.06
0.08
0.1
0.12
g_{app0}
T_{s_1}/T_{s_0}=red
T_{s_2}/T_{s_0}=blue

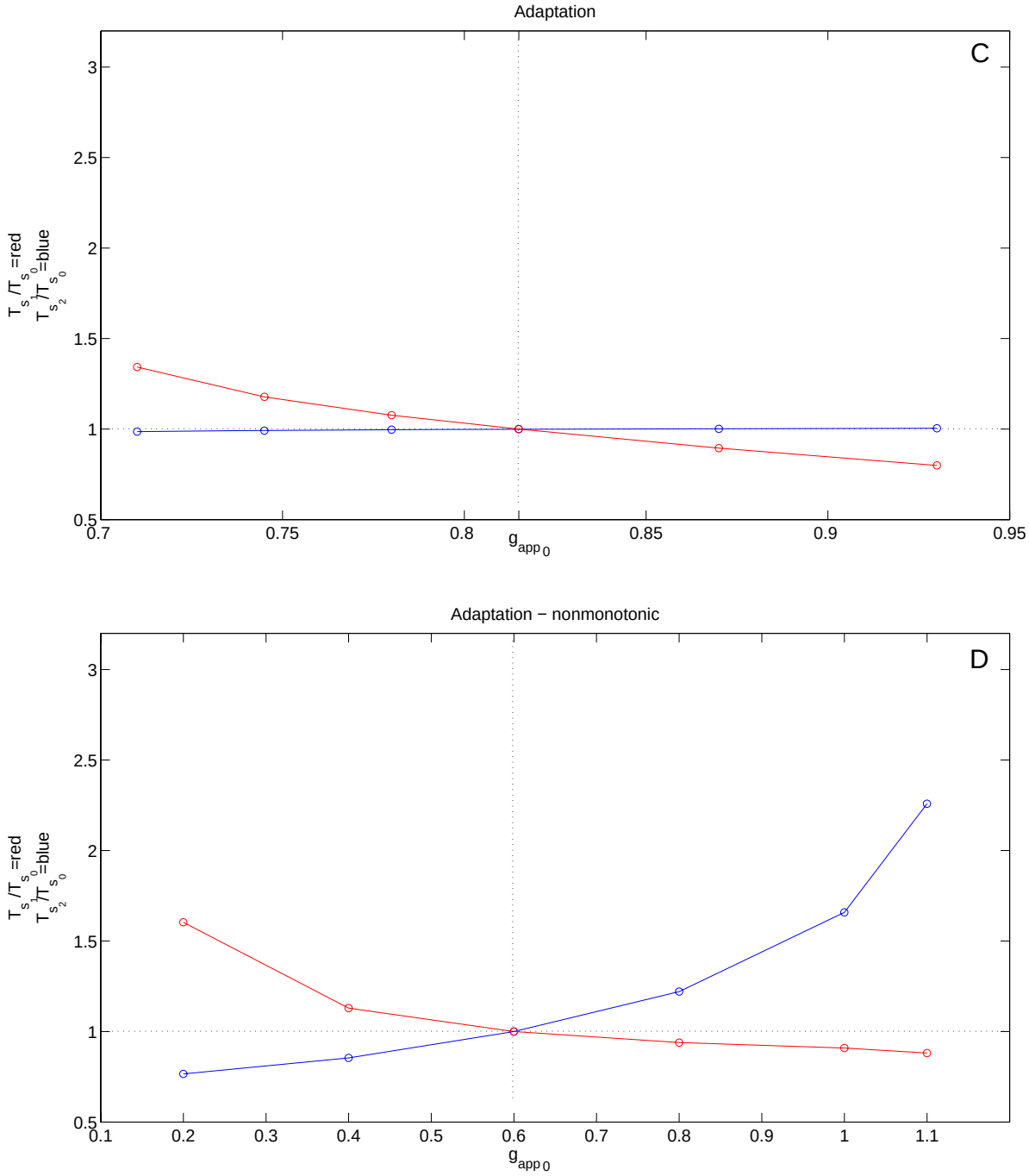

Figure 5: *Changes in silent phase durations with changes in g_{app_1}, the drive to cell 1. In each plot, g_{app_2} was held fixed at g_{app_0}, the baseline drive for the corresponding model, and g_{app_1} was varied above and below that level. T_{s_1} and T_{s_2} denote the resulting silent phase durations of cells 1 and 2, respectively, and T_{s_0} denotes the silent phase duration with $g_{app_1} = g_{app_2} = g_{app_0}$. Half-center oscillations based on (A) persistent sodium, (B) postinhibitory rebound, and (C) adaptation, Case 1, (D) adaptation, Case 2.*

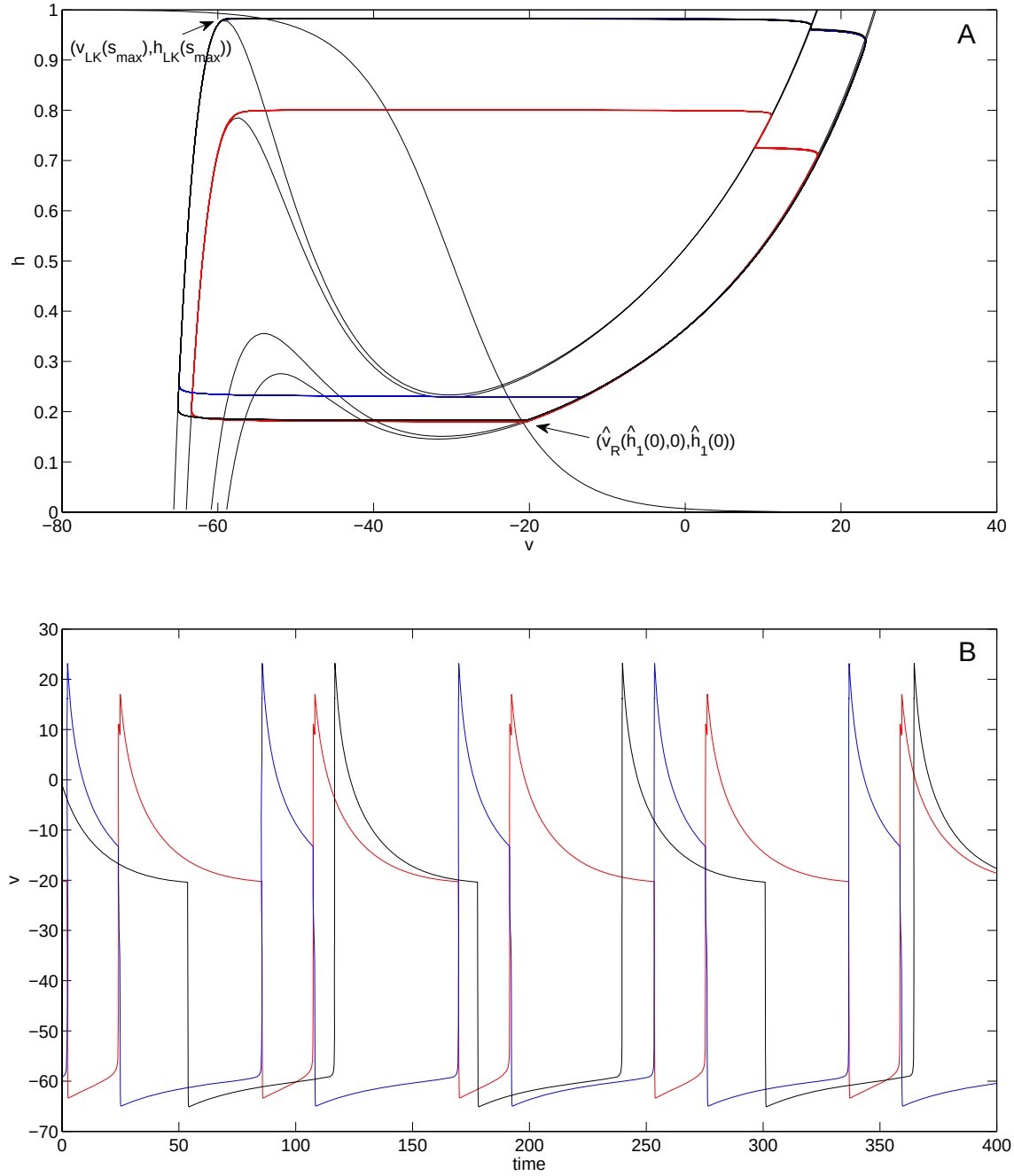

Figure 6: *Periodic oscillations in the model with persistent sodium, in the asymmetric case. An increase in the drive to cell* 1 *(red) decreases the duration of its silent phase and therefore the duration of the active phase of cell* 2 *(blue). The duration of the active phase of cell* 1*, and therefore the duration of the silent phase of cell* 2*, is only slightly affected. (A) Phase plane orbits. (B) Voltage time courses.*

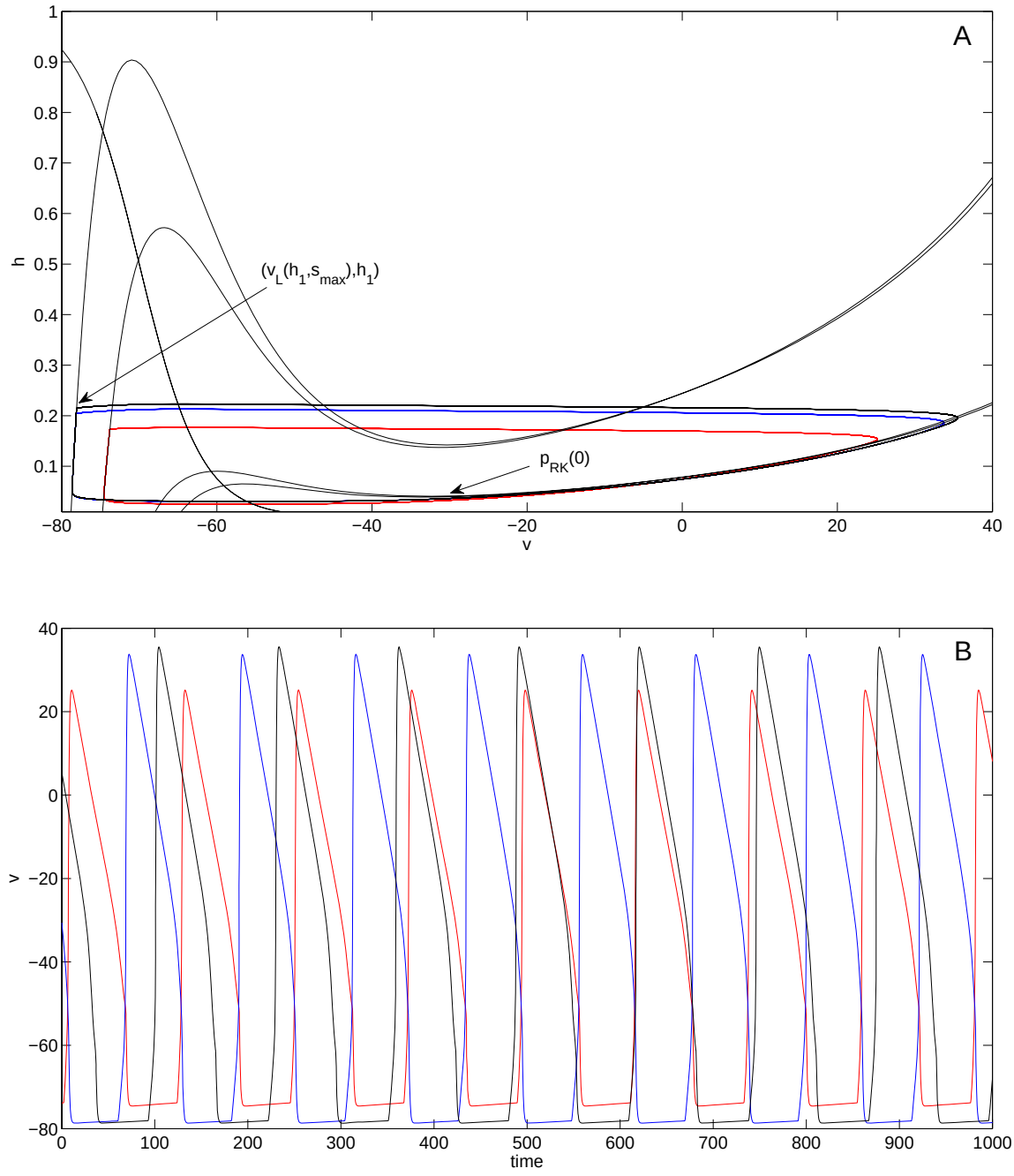

Figure 7: *Periodic oscillations in the model with postinhibitory rebound, in the asymmetric case. Both cell* 1*, with increased drive (red), and cell* 2 *have shorter active phases and therefore also shorter silent phases than in the balanced case. (A) Phase plane orbits. (B) Voltage time courses.*

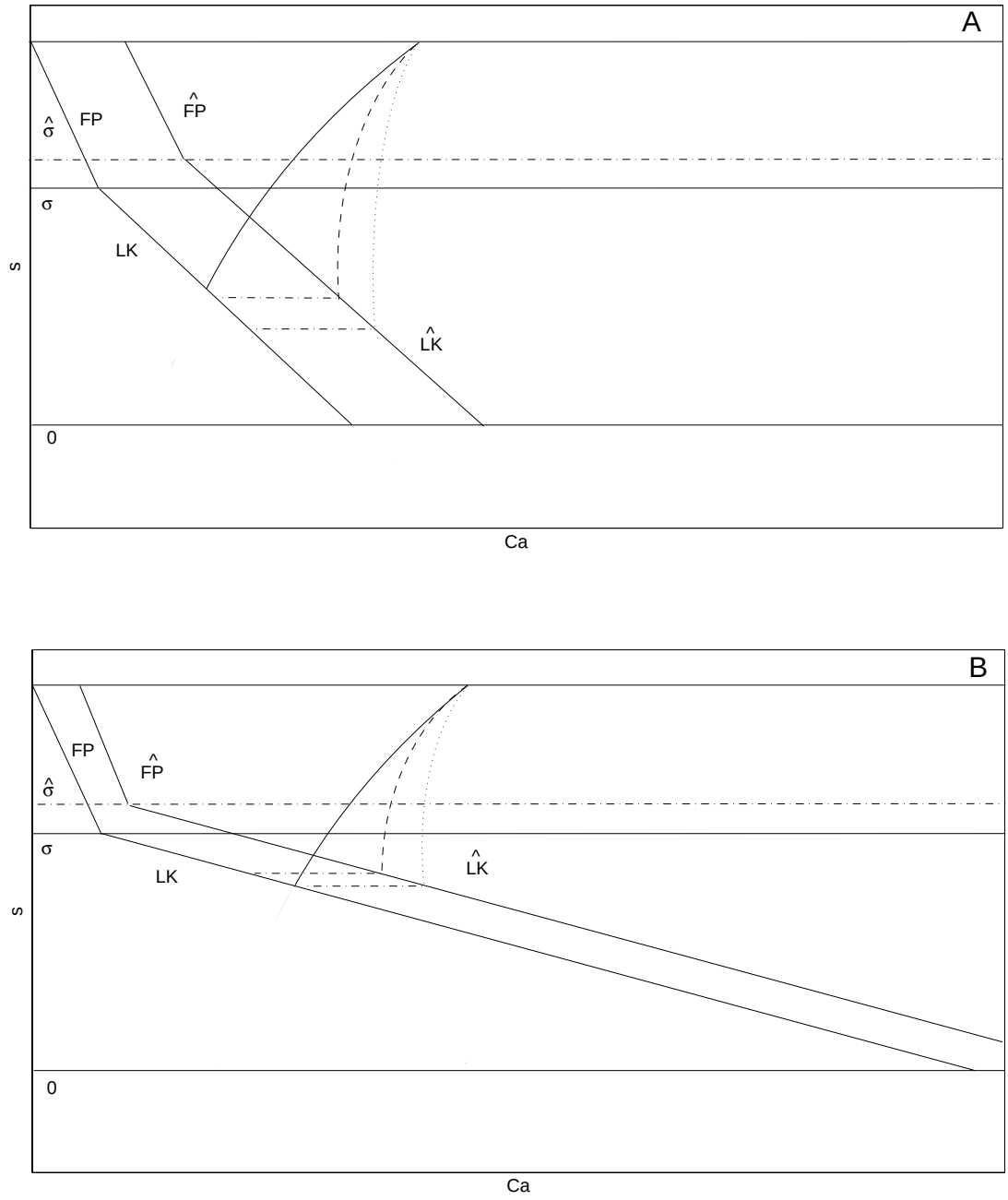

Figure 8: (Ca, s) *phase plane for the adaptation model. The structures (fixed points, FP, and left knees, LK) defined when drive is increased are labeled with the* $\wedge$ *symbol;* $\sigma, \hat{\sigma}$ *denote the* s *values at which FP and LK intersect with baseline and increased drive, respectively. The duration of the silent phase is dependent on how* $\dot{Ca}$ *and* Ca_{LK} *change with* g_{app}*, as well as on* $|\partial Ca_{LK}/\partial s|$*. (A) A small* $|\partial Ca_{LK}/\partial s|$ *promotes a long silent phase, with relatively high sensitivity to changes in* $\dot{Ca}$ *(dashed and dotted curves), seen as large changes in the* s*-value at which the trajectory reaches* $\hat{LK}$ *with changes in* $\dot{Ca}$*. (B) A large* $|\partial Ca_{LK}/\partial s|$ *promotes a short silent phase, with relatively low sensitivity to changes in* $\dot{Ca}$ *(dashed and dotted curves), seen as small changes in the* s*-value at which the trajectory reaches* $\hat{LK}$ *with changes in* $\dot{Ca}$*.*

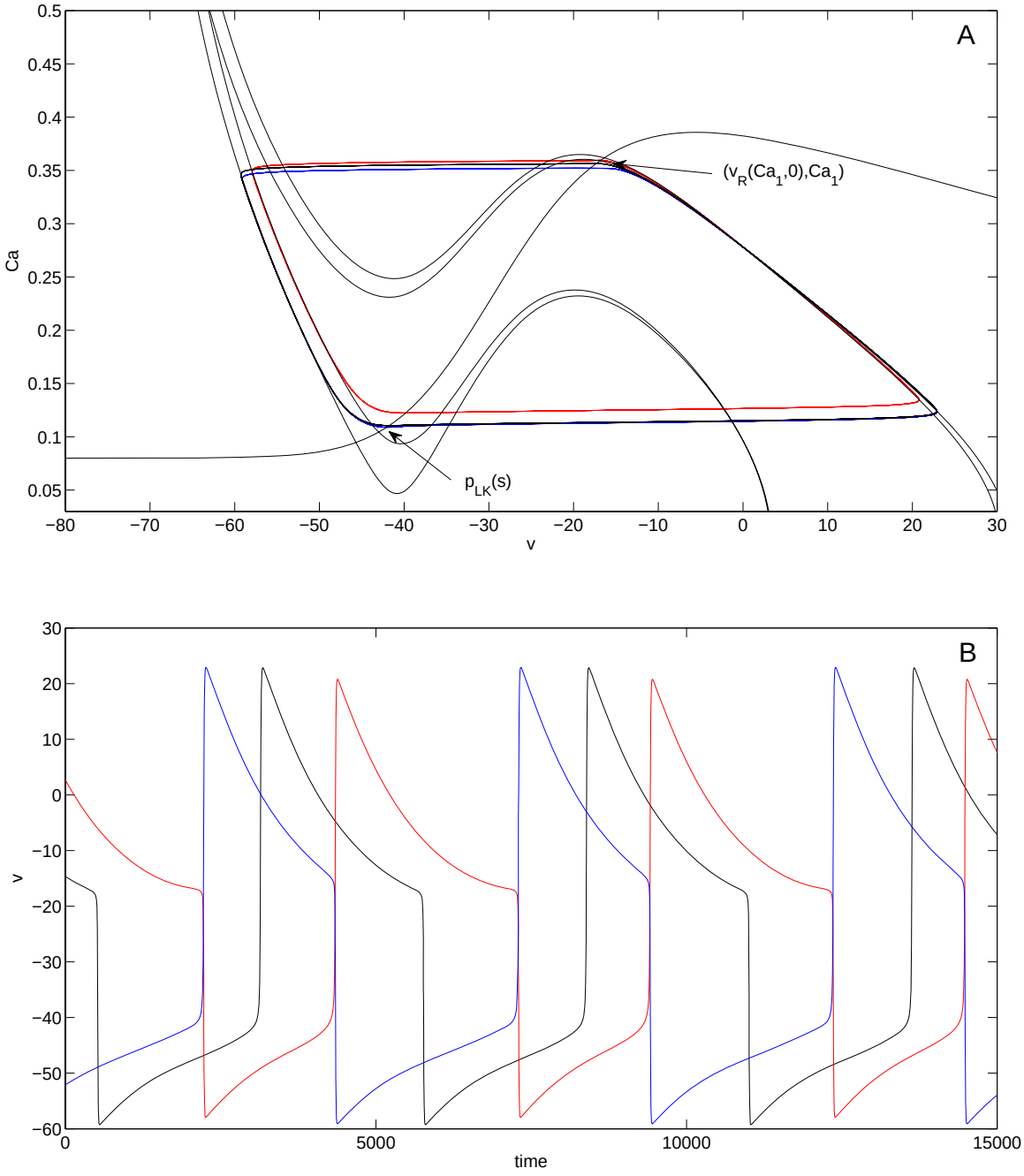

Figure 9: *Periodic oscillations in the model with adaptation (Case 1), with asymmetric drive. Extra drive to cell* 1 *(red) causes it to have a shorter silent phase and longer active phase, while cell* 2 *(blue), with baseline drive, has a shorter active phase and longer silent phase, correspondingly. (A) Phase plane orbits. (B) Voltage time courses.*

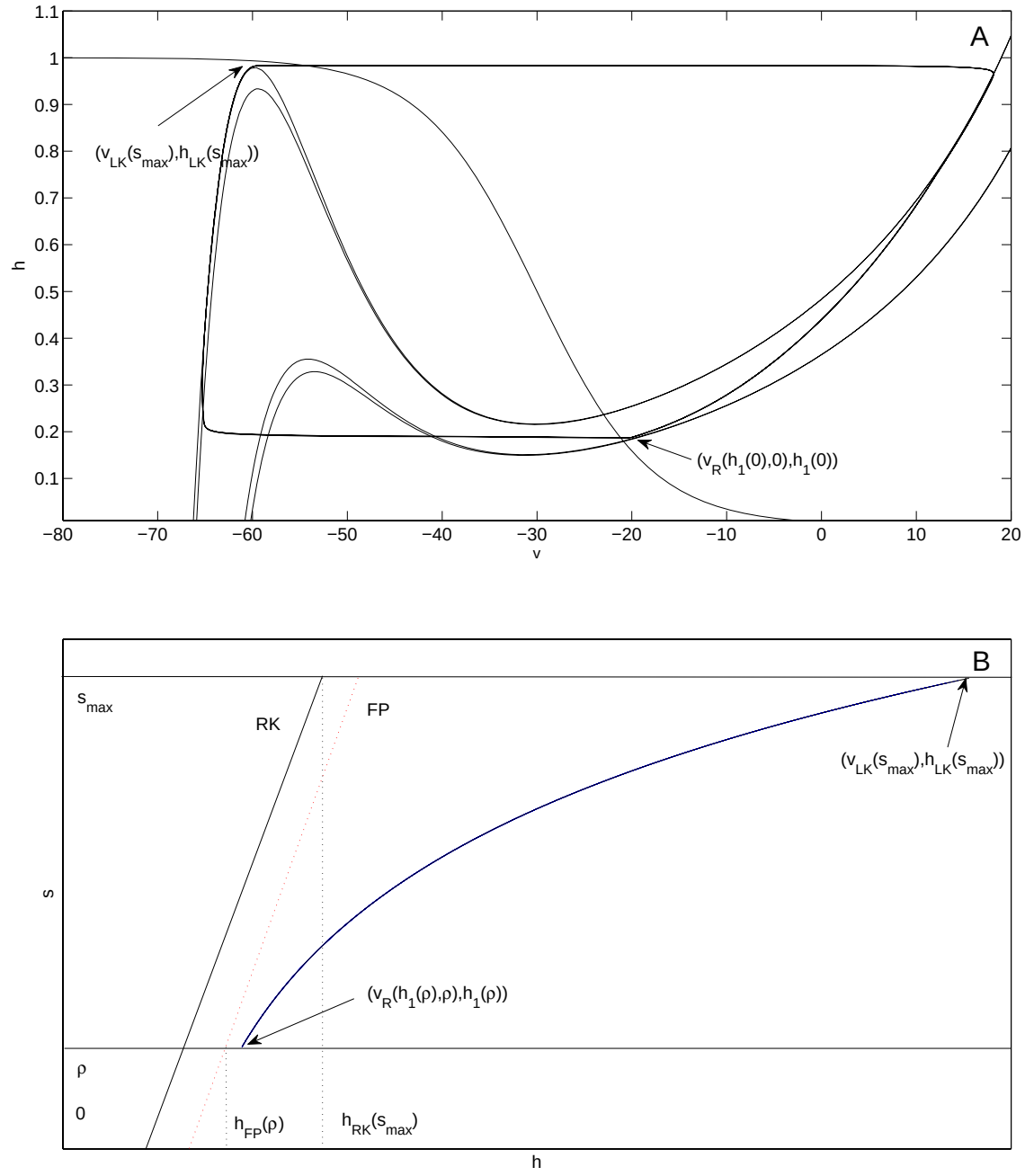

Figure 10: *Periodic oscillations in the model with persistent sodium, with slow synaptic decay and with balanced drive. (A) Basic period orbit. (B) Slow phase plane for the active phase.*

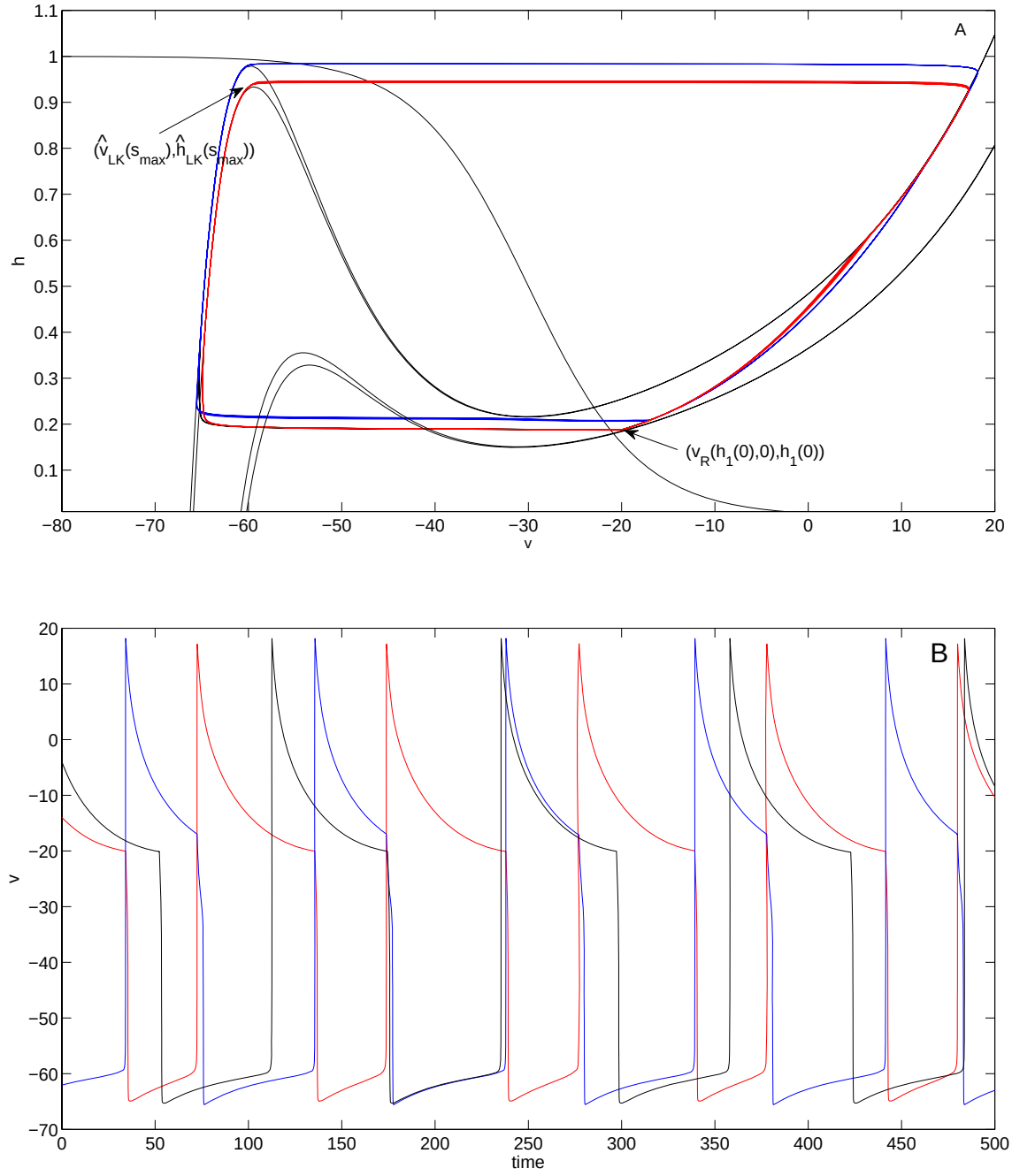

Figure 11: *Periodic oscillations in the model with persistent sodium, with slow synaptic decay and asymmetric drive. An increase in the drive to cell* 1 *(red) decreases the duration of its silent phase and therefore of the active phase of cell* 2 *(blue). The silent phase of cell* 2 *and thus the active phase of cell* 1 *do not decrease significantly. (A) Phase plane orbits. (B) Voltage time courses.*

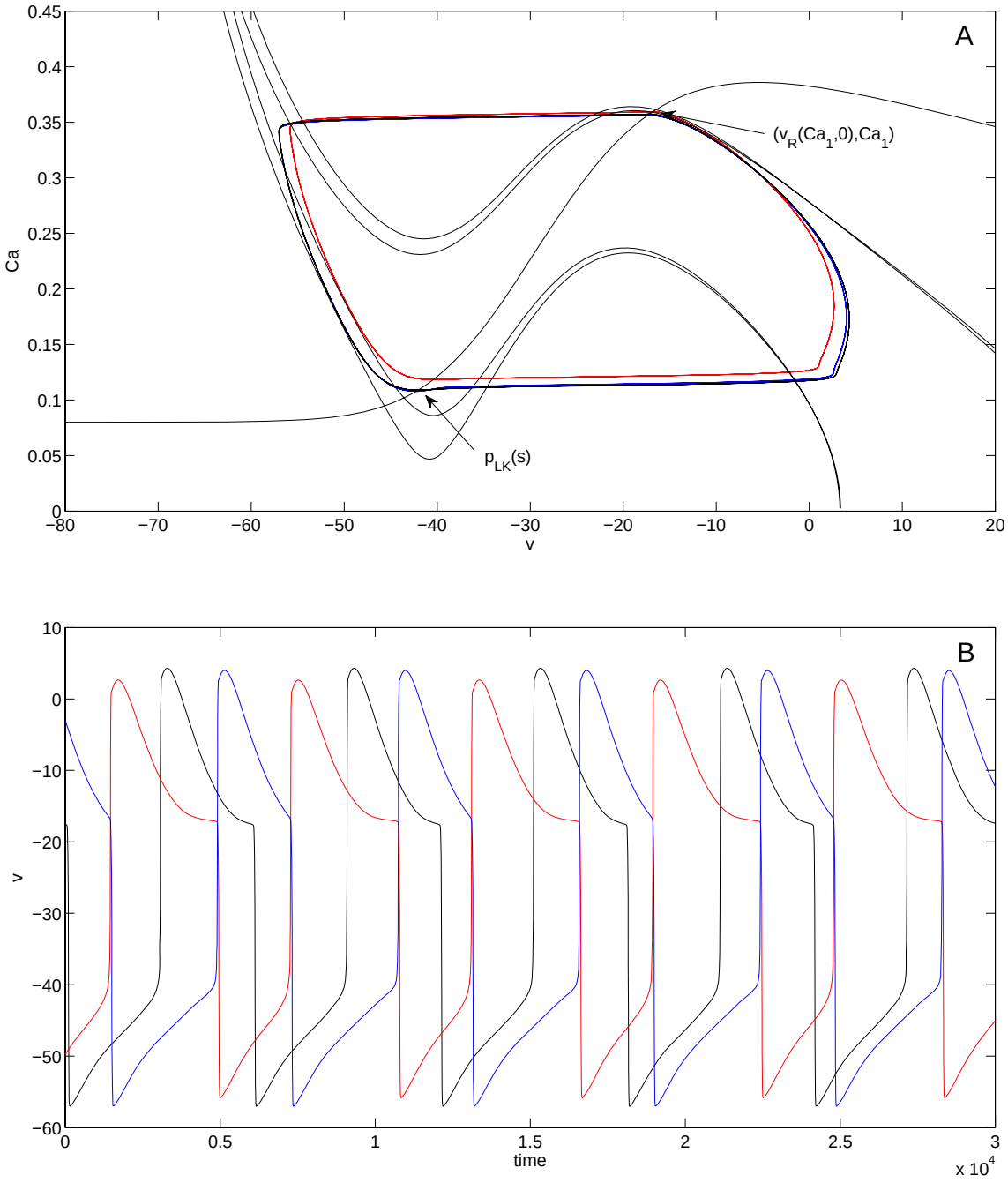

Figure 12: *Periodic oscillations in the model with adaptation (Case 1), with slow synaptic decay and asymmetric drive. As in the fast synaptic decay case, an increase in the drive to cell 1 (red) decreases its silent and increases its active phase duration, with corresponding changes in the phase durations of cell 2 (blue). (A) Phase plane orbits. (B) Voltage time courses.*

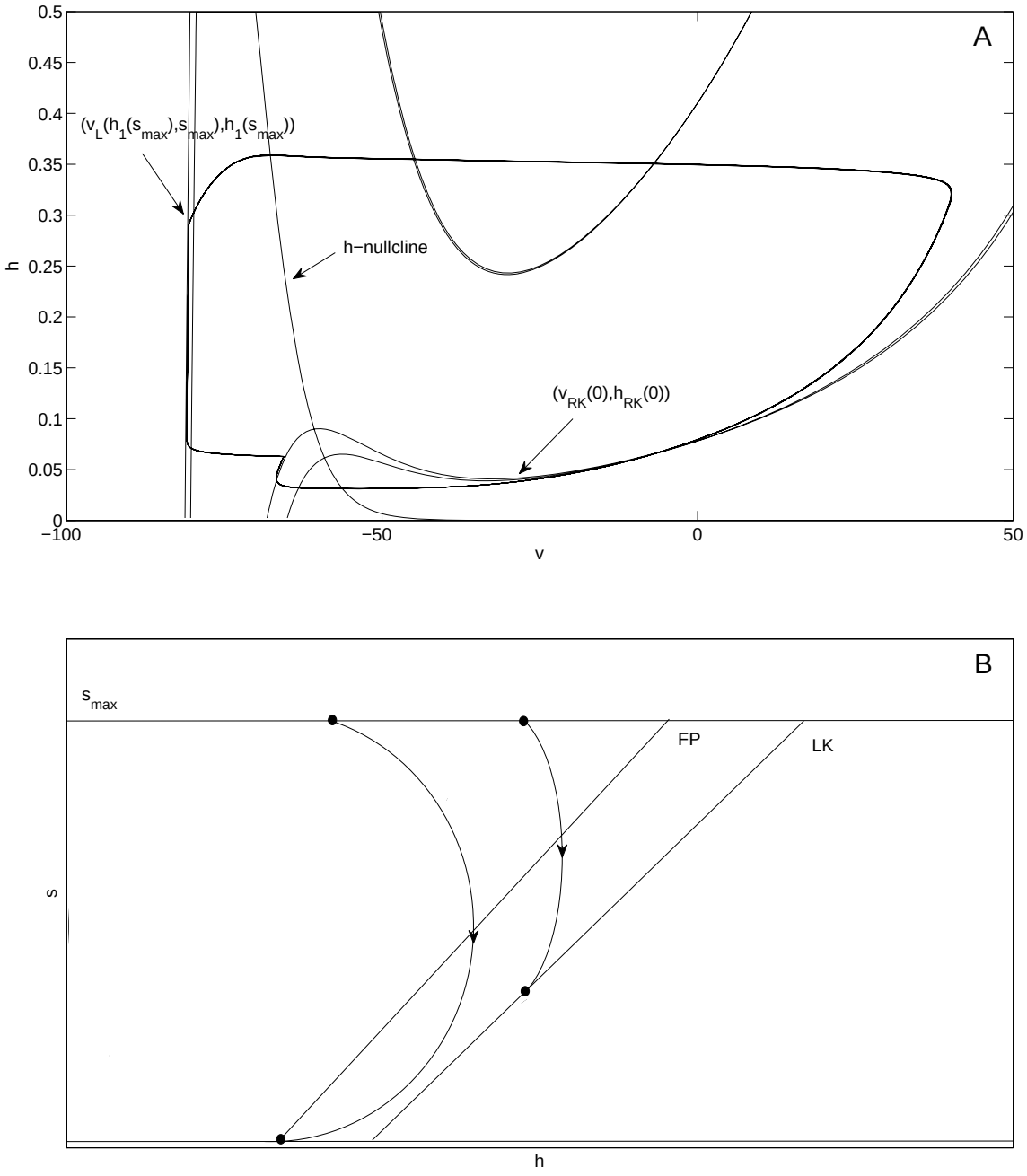

Figure 13: *Periodic oscillations in the model with postinhibitory rebound, with slow synaptic decay and balanced drive. (A) Basic period orbit in the (v, h) phase plane. (B) Slow phase plane. Whether the cell in the silent phase is able to reach the curve of left knees depends on the relative rates of change of its h–coordinate and of the inhibition it receives.*

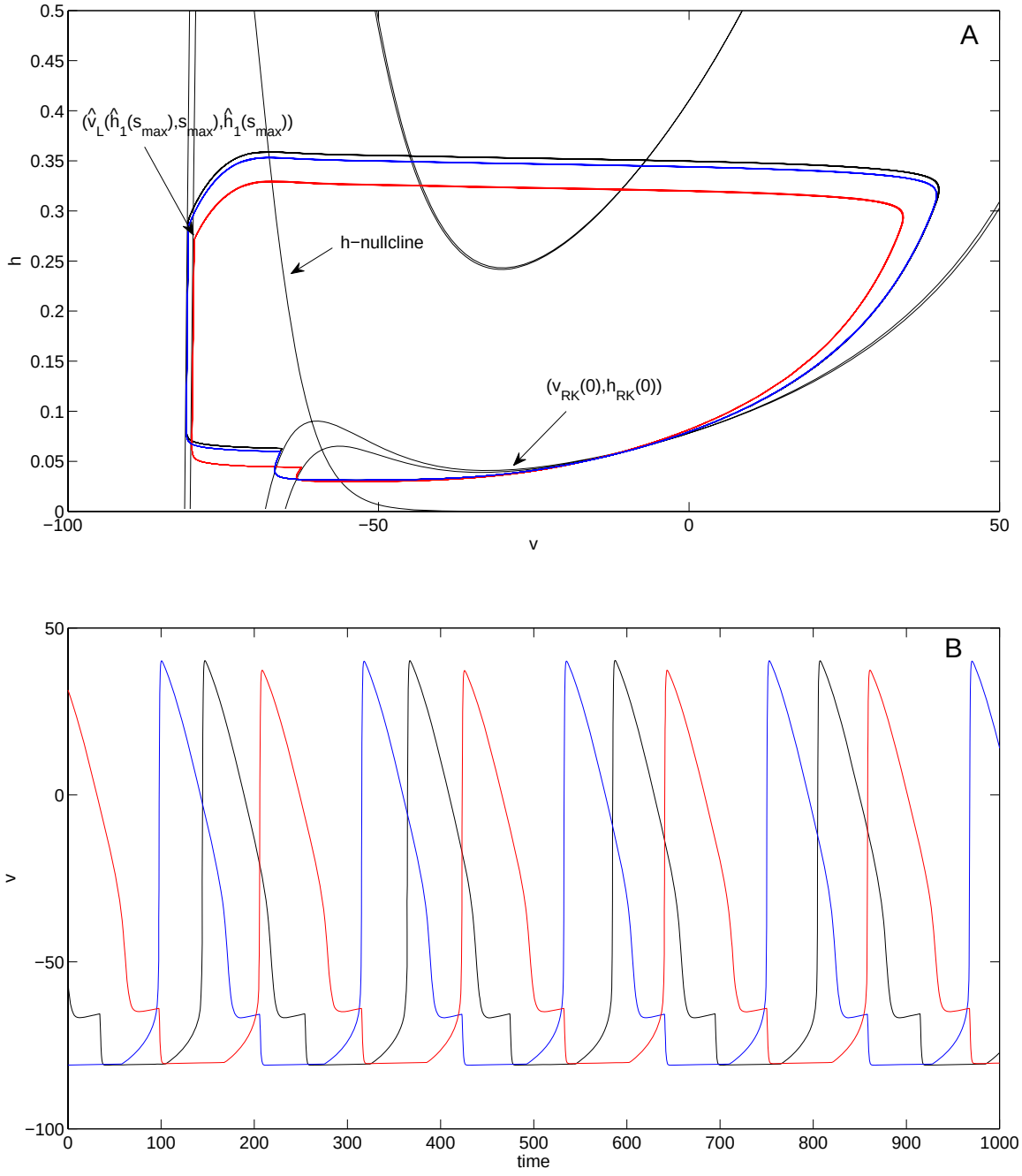

Figure 14: *Periodic oscillations in the model with postinhibitory rebound, with slow synaptic decay and asymmetric drive. An increase in the drive to cell* 1 *(red) slightly decreases its silent and active phase durations and changes the phase durations of cell* 2 *(blue) correspondingly. (A) Phase plane orbits. (B) Voltage time courses.*

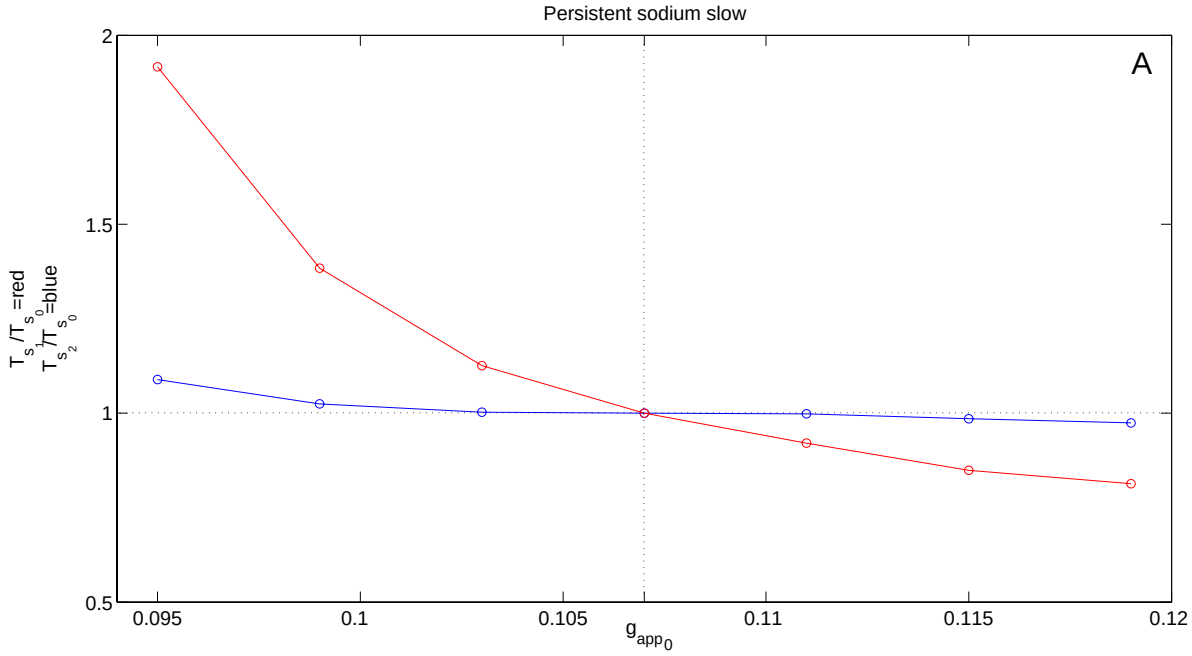
Persistent sodium slow
A
2
1.5
1
0.5
0.095
0.1
0.105
0.11
0.115
0.12
g_{app_0}
T_{s_1}/T_{s_0}=red
T_{s_2}/T_{s_0}=blue

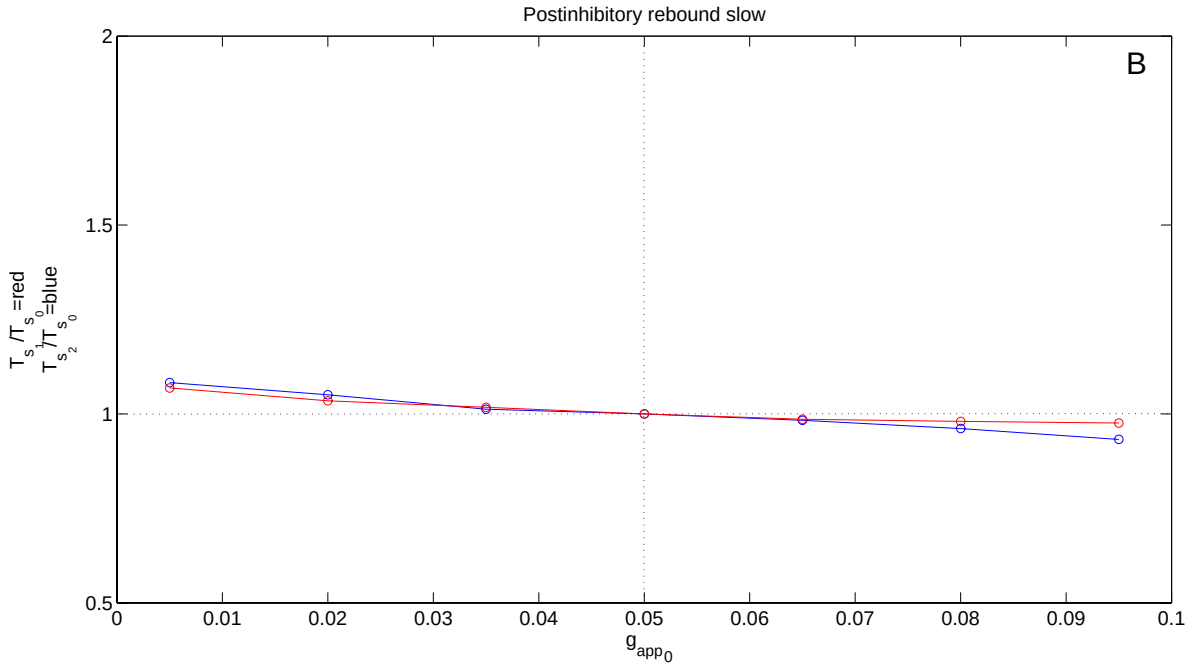
Postinhibitory rebound slow
B
2
1.5
1
0.5
0
0.01
0.02
0.03
0.04
0.05
0.06
0.07
0.08
0.09
0.1
g_{app_0}
T_{s_1}/T_{s_0}=red
T_{s_2}/T_{s_0}=blue

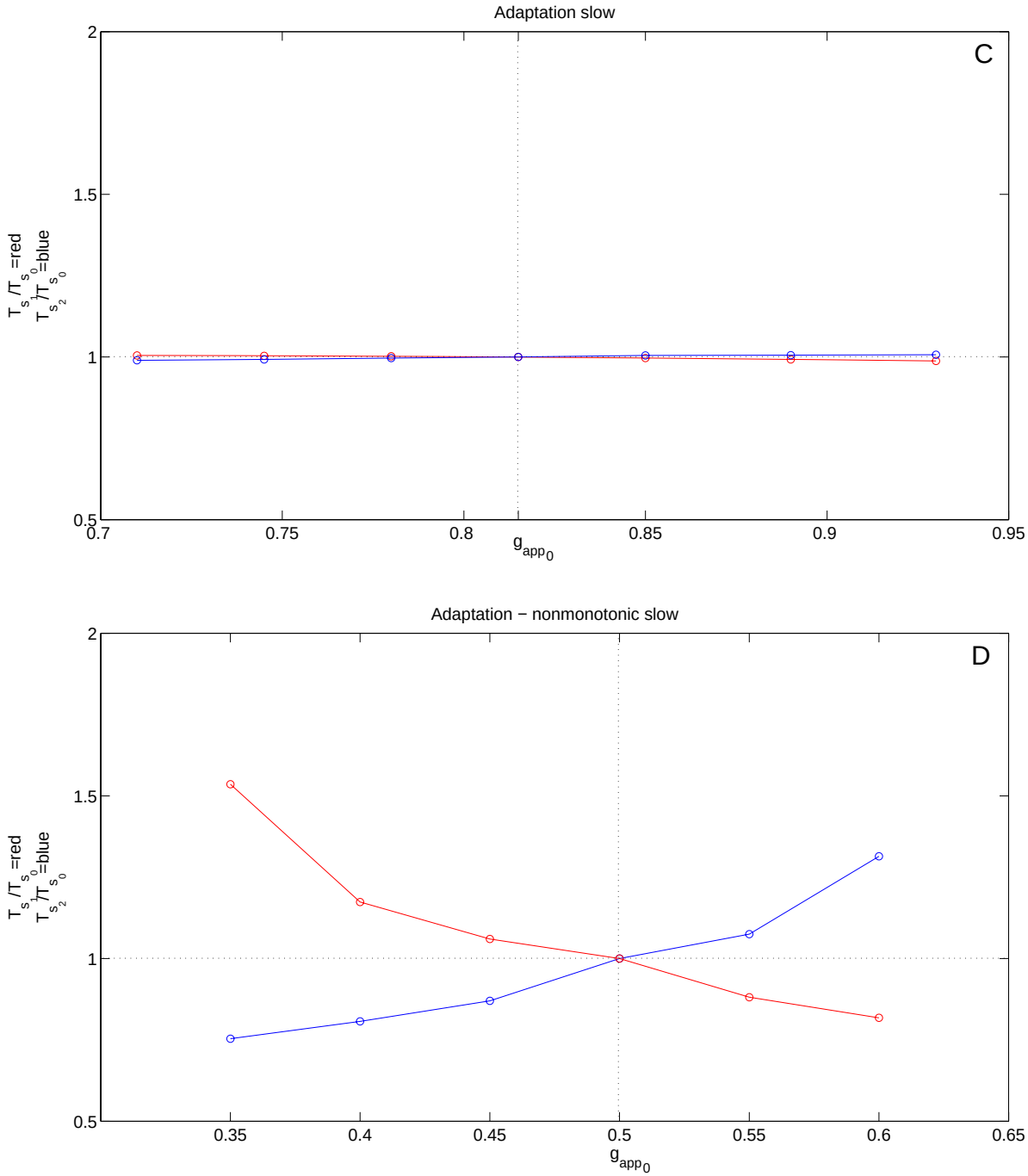

Figure 15: *Changes in silent phase durations dependent on increased drive to cell* 1 *(drive to cell* 2 *has not been changed) in the persistent sodium, postinhibitory rebound and the two adaptation cases with slow decay of inhibition. In each plot,* g_{app_2} *was held fixed at* g_{app_0}*, the baseline drive for the corresponding model, and* g_{app_1} *was varied above and below that level.* T_{s_1} *and* T_{s_2} *denote the silent phase durations of cell* 1 *and* 2*, respectively and* T_{s_0} *denotes the silent phase duration of the basic periodic orbits shown in subsection 2.2.*

References

[1] T. Brown, *The Intrinsic Factors in the Act of Progression in the Mammal*, Proc. Roy. Soc. London. Series B., 84 (1911), pp. 308–319.

[2] ——, *On the nature of the fundamental activity of the nervous centres; together with an analysis of the conditioning of rhythmic activity in progression, and a theory of the evolution of function in the nervous system*, J. Physiol., 48 (1914), p. 18.

[3] R. Butera, J. Rinzel, and J. Smith, *Models of respiratory rhythm generation in the pre-Bötzinger complex. I. Bursting pacemaker neurons*, J. Neurophysiol., **81** (1999), pp. 382–397.

[4] R. Calabrese, *Half-center oscillators underlying rhythmic movements*, in The Handbook of Brain Theory and Neural Networks, M. Arbib, ed., MIT Press, Cambridge, MA, 1995, pp. 444–447.

[5] S. Grillner, *Neurobiological bases of rhythmic motor acts in vertebrates*, Science, 228 (1985), pp. 143–149.

[6] ——, *Biological Pattern Generation: The Cellular and Computational Logic of Networks in Motion*, Neuron, 52 (2006), pp. 751–766.

[7] J. Halbertsma, *The stride cycle of the cat: the modelling of locomotion by computerized analysis of automatic recordings.*, Acta Physiol. Scand. Suppl., 521 (1983), pp. 1–75.

[8] R. Harris-Warrick, *Pattern generation.*, Curr. Opin. Neurobiol., 3 (1993), pp. 982–8.

[9] E. Izhikevich, *Dynamical Systems in Neuroscience: The Geometry of Excitability and Bursting*, MIT Press, Cambridge, MA, 2006.

[10] M. Lafreniere-Roula and D. McCrea, *Deletions of Rhythmic Motoneuron Activity During Fictive Locomotion and Scratch Provide Clues to the Organiza-*

tion of the Mammalian Central Pattern Generator, J. Neurophysiol., 94 (2005), pp. 1120–1132.

[11] A. Lundberg, *Half-centres revisited*, in Regulatory Functions of the CNS. Motion and Organization Principles, J. Szentagothai, M. Palkovits, and J. Hamori, eds., Pergamon Akadem Kiado, Budapest, 1981, pp. 155–167.

[12] E. Marder, *Motor pattern generation*, Curr. Opin. Neurobiol., 10 (2000), pp. 691–698.

[13] E. Marder and D. Bucher, *Central pattern generators and the control of rhythmic movements*, Current Biology, 11 (2001), pp. 986–996.

[14] E. Marder, D. Bucher, D. Schulz, and A. Taylor, *Invertebrate Central Pattern Generation Moves along*, Current Biology, 15 (2005), pp. 685–699.

[15] E. Marder and R. Calabrese, *Principles of rhythmic motor pattern generation*, Physiol. Rev., **76** (1996), pp. 687–717.

[16] K. Matsuoka, *Mechanisms of frequency and pattern control in the neural rhythm generators*, Biol. Cybern., 56 (1987), pp. 345–353.

[17] D. McCrea and I. Rybak, *Modeling the mammalian locomotor CPG: insights from mistakes and perturbations.*, Prog. Brain. Res., 165 (2007), pp. 235–53.

[18] E. Mischenko, Y. Kolesov, A. Kolesov, and N. Rozov, *Asymptotic Methods in Singularly Perturbed Systems*, Plenum Publishing Corporation, New York, 1994.

[19] A. Olypher, G. Cymbalyuk, and R. Calabrese, *Hybrid systems analysis of the control of burst duration by ed calcium current in leech heart interneurons*, J. Neurophysiol., **96** (2006), pp. 2857–2867.

[20] G. Orlovskiĭ, T. Deliagina, and S. Grillner, *Neuronal Control of Locomotion: From Mollusc to Man*, Oxford University Press, 1999.

[21] P. Rowat and A. Selverston, *Modeling the gastric mill central pattern generator of the lobster with a relaxation-oscillator network*, J. Neurophysiol., 70 (1993), pp. 1030–1053.

[22] J. Rubin, *Bursting induced by excitatory synaptic coupling in non-identical conditional relaxation oscillators or square-wave bursters*, Phys. Rev. E, **74** (2006), p. 021917.

[23] J. Rubin and D. Terman, *Geometric singular perturbation analysis of neuronal dynamics*, in Handbook of Dynamical Systems, vol. 2: Towards Applications, B. Fiedler, ed., Elsevier, 2002.

[24] J. Rubin and D. Terman, *High frequency stimulation of the subthalamic nucleus eliminates pathological thalamic rhythmicity in a computational model*, J. Comp. Neurosci., **16** (2004), pp. 211–235.

[25] I. Rybak, N. Shevtsova, M. Lafreniere-Roula, and D. McCrea, *Modelling spinal circuitry involved in locomotor pattern generation: insights from deletions during fictive locomotion*, J. Physiol., 577 (2006), pp. 617–639.

[26] A. Selverston and M. Moulins, *Oscillatory Neural Networks*, Ann. Rev. Physiol., 47 (1985), pp. 29–48.

[27] A. Shpiro, R. Curtu, J. Rinzel, and N. Rubin, *Dynamical characteristics common to neuronal competition models*, J. Neurophysiol., **97** (2007), pp. 462–473.

[28] M. Sirota and M. Shik, *The cat locomotion elicited through the electrode implanted in the mid-brain*, Sechenov Physiol. J. USSR, 59 (1973), pp. 1314–1321.

[29] F. Skinner, N. Kopell, and E. Marder, *Mechanisms for oscillation and frequency control in reciprocally inhibitory model neural networks*, J. Comput. Neurosci., 1 (1994), pp. 69–87.

[30] F. Skinner, G. Turrigiano, and E. Marder, *Frequency and burst duration in oscillating neurons and two-cell networks*, Biol. Cybern., 69 (1993), pp. 375–383.

[31] V. Sohal and J. Huguenard, *Reciprocal inhibition controls the oscillatory state in thalamic networks*, Neurocomp., **44** (2002), pp. 653–659.

[32] D. Somers and N. Kopell, *Rapid synchronization through fast threshold modulation*, Biol. Cybern., **68** (1993), pp. 393–407.

[33] M. Sorensen, S. DeWeerth, G. Cymbalyuk, and R. Calabrese, *Using a hybrid neural system to reveal regulation of neuronal network activity by an intrinsic current*, J. Neurosci., **24** (2004), pp. 5427–5438.

[34] J. Tabak, M. O'Donovan, and J. Rinzel, *Differential control of active and silent phases in relaxation models of neuronal rhythms*, J. Comp. Neurosci., **21** (2006), pp. 307–328.

[35] A. Taylor, G. Cottrell, and W. Kristan, Jr., *Analysis of oscillations in a reciprocally inhibitory network with synaptic depression*, Neural. Comput., **14** (2002), pp. 561–581.

[36] S. Tazerart, J. Viemari, P. Darbon, L. Vinay, and F. Brocard, *Contribution of Persistent Sodium Current to Locomotor Pattern Generation in Neonatal Rats*, J. Neurophysiol., 98 (2007), p. 613.

[37] X. Wang and J. Rinzel, *Alternating and Synchronous Rhythms in Reciprocally Inhibitory Model Neurons*, Neural Comput., 4 (1992), pp. 84–97.

[38] S. Yakovenko, D. McCrea, K. Stecina, and A. Prochazka, *Control of Locomotor Cycle Durations*, J. Neurophysiol., 94 (2005), pp. 1057–1065.

[39] G. Zhong, M. Masino, and R. Harris-Warrick, *Persistent Sodium Currents Participate in Fictive Locomotion Generation in Neonatal Mouse Spinal Cord*, J. Neurosci., 27 (2007), p. 4507.